

RESEARCH ARTICLE

A new paradigm for leprosy diagnosis based on host gene expression

Thyago Leal-Calvo¹, Charlotte Avanzi^{2aa}, Mayara Abud Mendes¹, Andrej Benjak^{2ab}, Philippe Busso², Roberta Olmo Pinheiro¹, Euzenir Nunes Sarno¹, Stewart Thomas Cole^{2,3}, Milton Ozório Moraes^{1*}

1 Laboratório de Hanseníase, Instituto Oswaldo Cruz, FIOCRUZ, Rio de Janeiro, Rio de Janeiro, Brazil, **2** Global Health Institute, École Polytechnique Fédérale de Lausanne, Lausanne, Switzerland, **3** Institut Pasteur, Paris, France

^{aa} Current address: Department of Microbiology, Immunology and Pathology, Mycobacteria Research Laboratories, Colorado State University, Fort Collins, Colorado, United States of America

^{ab} Current address: Department for BioMedical Research, Oncogenomics Laboratory, University of Bern, Bern, Switzerland

* milton.moraes@fiocruz.br



OPEN ACCESS

Citation: Leal-Calvo T, Avanzi C, Mendes MA, Benjak A, Busso P, Pinheiro RO, et al. (2021) A new paradigm for leprosy diagnosis based on host gene expression. PLoS Pathog 17(10): e1009972. <https://doi.org/10.1371/journal.ppat.1009972>

Editor: Erwin Schurr, McGill University, CANADA

Received: June 29, 2021

Accepted: September 28, 2021

Published: October 25, 2021

Copyright: © 2021 Leal-Calvo et al. This is an open access article distributed under the terms of the [Creative Commons Attribution License](https://creativecommons.org/licenses/by/4.0/), which permits unrestricted use, distribution, and reproduction in any medium, provided the original author and source are credited.

Data Availability Statement: All raw and processed data plus computer source code are available in the following repositories: EMBL-EBI ENA: <https://www.ebi.ac.uk/ena/browser/view/ERP128243> EMBL-EBI ArrayExpress: <https://www.ebi.ac.uk/arrayexpress/experiments/E-MTAB-10318/>. Zenodo: [10.5281/zenodo.4682010](https://zenodo.org/record/4682010).

Funding: The first author (TLC) was supported by a PhD scholarship from Conselho Nacional de Desenvolvimento Científico e Tecnológico, CNPq, <https://www.gov.br/cnpq/pt-br>. This work was also supported by the Fundação Carlos Chagas Filho de Amparo à Pesquisa do Estado do Rio de Janeiro,

Abstract

Transcriptional profiling is a powerful tool to investigate and detect human diseases. In this study, we used bulk RNA-sequencing (RNA-Seq) to compare the transcriptomes in skin lesions of leprosy patients or controls affected by other dermal conditions such as granuloma annulare, a confounder for paucibacillary leprosy. We identified five genes capable of accurately distinguishing multibacillary and paucibacillary leprosy from other skin conditions. Indoleamine 2,3-dioxygenase 1 (*IDO1*) expression alone was highly discriminatory, followed by *TLR10*, *BLK*, *CD38*, and *SLAMF7*, whereas the *HS3ST2* and *CD40LG* mRNA separated multi- and paucibacillary leprosy. Finally, from the main differentially expressed genes (DEG) and enriched pathways, we conclude that paucibacillary disease is characterized by epithelioid transformation and granuloma formation, with an exacerbated cellular immune response, while multibacillary leprosy features epithelial-mesenchymal transition with phagocytic and lipid biogenesis patterns in the skin. These findings will help catalyze the development of better diagnostic tools and potential host-based therapeutic interventions. Finally, our data may help elucidate host-pathogen interplay driving disease clinical manifestations.

Author summary

Despite effective treatment, leprosy is still a significant public health issue in more than 120 countries, with more than 200 000 new cases yearly. The disease is caused mainly by *Mycobacterium leprae*, a slow-growing bacillus still uncultivable in axenic media. This limitation has hampered basic research into host-pathogen interaction and the development of new diagnostic assays. Currently, leprosy is diagnosed clinically, with no standalone diagnostic assay accurate enough for all clinical forms. Here, we use RNA-seq transcriptome profiling in leprosy lesions and granuloma annulare to identify mRNA biomarkers

FAPERJ, grant no. 04/2015, <http://www.faperj.br/>; Cooperação Bilateral CB-FAPERJ/SNSF (MOM); the Fondation Raoul Follereau (STC), <https://www.raoul-follereau.org/>; Swiss National Science Foundation grants IZRJZ3_164174 (STC), <https://www.snf.ch/en>; and the Heiser Program of the New York Community Trust for Research in Leprosy, grant no. P18-000250 (MOM and CA), <https://www.nycommunitytrust.org/>. The funders had no role in study design, data collection and analysis, decision to publish, or preparation of the manuscript.

Competing interests: The authors have declared that no competing interests exist.

with potential diagnostic applications. Also, we explored new pathways that can be useful in further understanding the host-pathogen interaction and how the bacteria bypass host immune defenses. We found that *IDOI*, a gene involved with tryptophan catabolism, is an excellent candidate for distinguishing leprosy lesions from other dermatoses. Additionally, we observed that a previous signature of keratinocyte development and cornification negatively correlates with epithelial-mesenchymal transition genes in the skin, suggesting new ways in which the pathogen may subvert its host to survive and spread throughout the body. Our study identifies new mRNA biomarkers that can improve leprosy diagnostics and describe new insights about host-pathogen interactions in human skin.

Introduction

Leprosy is a chronic infectious disease caused mainly by the slow-growing intracellular pathogen *Mycobacterium leprae* that does not grow in axenic media. This bacterium resides preferentially in skin macrophages and Schwann cells in peripheral nerves, inducing dermatosis and/or neuritis. Patients can present several distinct clinical forms according to their immune response, histopathological characterization, and bacterial load. A localized tuberculoid form (TT) is characterized by low bacterial counts and a strong cellular immune response. Conversely, in the opposite lepromatous (LL) pole, a disseminated form, patients exhibit several lesions, a predominantly humoral response, and a high bacterial load in the tissues [1–3]. Borderline forms are classified according to their proximity to the poles. For operational and treatment purposes, leprosy is classified by the World Health Organization as paucibacillary (PB) or multibacillary (MB), based on the number of skin lesions, association with nerve involvement or the bacilli detection in slit-skin smears [4].

Early and precise diagnosis is instrumental to leprosy control since delay in diagnosis leads to late multidrug therapy, higher disability risk, and continuing transmission, as highlighted by the 200,000 new cases consistently reported annually in the last 10 years [4,5]. However, bacteriological, immunological, genetics or molecular methods are not sufficient for specific diagnosis when used alone. Diagnosis most commonly relies on clinical evaluation, occasionally complemented with histopathological examination and bacterial counts, but these procedures are mostly performed in national reference centers [4,6].

Efforts have been deployed to improve leprosy diagnostics using cutting-edge technologies, such as molecular identification of *M. leprae*, serological tests for specific bacterial antigens, and quantification of host biomarkers in plasma or *in vitro* whole blood assays (WBA) [7–9]. Overall, all methods outperform standard clinical diagnosis and can compensate for the low accuracy in detecting PB patients [4,7,8,10–14]. Yet, until now such investigations involved comparing confirmed leprosy cases against healthy endemic controls, who are not representative of individuals with suspected leprosy. Here, other skin conditions represent a better comparator.

Identification of markers for early infection is hindered by our poor understanding of pathogenicity and the mechanism by which patients develop one or the other form of leprosy, and nerve injuries [15]. Gene expression signatures have been used as diagnostic tools for several illnesses, from infectious [10–12,14] and autoimmune diseases [16,17] to cancer [18–20]. Some signatures have already been approved for clinical use [12,21–23]. In leprosy, findings from past studies indicate the great potential of expression profiling for disease diagnosis [24–27]. Nonetheless, they were limited by the number of patients [28], or lacked proper epidemiological controls, such as differential diagnosis groups.

Here, we applied a combination of bulk RNA sequencing and quantitative validation by RT-qPCR on RNA extracted from skin biopsies of various leprosy forms and from non-leprosy patients to define a specific leprosy host signature applicable to diagnosis. Then, we explored gene expression patterns to improve our understanding of the immunopathogenic mechanisms towards leprosy polarization.

Results

Discrimination of leprosy vs. non-leprosy lesions based on mRNA expression

RNA sequencing was used for pinpointing host candidate genes capable of differentiating leprosy lesions from one of the commonest differential diagnoses of leprosy, granuloma annulare (GA), and from healthy skin. RNA from skin lesions of all leprosy clinical forms ($n = 33$), plus GA ($n = 4$) and healthy skin ($n = 5$) were sequenced (S1 Table). Differentially expressed genes (DEG) in leprosy vs. non-leprosy (GA + healthy skin) samples resulted in 1160 DEG with a $|\log_2FC| \geq 1$ and $FDR \leq 0.01$, with 961 upregulated in leprosy forms compared to non-leprosy (Fig 1A, 1B and S2 Table). Exploratory hierarchical clustering of the DEG with $|\log_2FC| \geq 1$ and $FDR < 0.01$ grouped all patients' samples into roughly two clusters, except for two: one BL leprosy and one GA that clustered apart from samples with the same diagnosis (Fig 1C). Gene Ontology enrichment analysis of up-regulated genes in leprosy compared to non-leprosy showed enrichment for biological processes associated with leukocyte activation, T-cell activation, immune response, response to the bacterium, neutrophil degranulation, cell killing, cytokine secretion, purinergic receptor signaling pathway, and regulation of defense response to viruses by the host (Fig 1D and S3 Table).

A total of 15 genes with the largest effect size ($|\log_2FC| \geq 1.5$, $FDR < 0.001$), highest area under the curve (AUC), and plausible involvement with leprosy pathogenesis (S4 Table) were then validated using a two-step RT-qPCR with a new, larger, and more heterogeneous dataset including skin lesion samples from leprosy patients ($n = 25$), and other common dermatoses ($n = 23$) (S1 Table). Other dermatological diseases (ODD) included dermatitis ($n = 7$), eczema ($n = 1$), erythema ($n = 4$), GA ($n = 6$), lichen planus ($n = 2$), psoriasis ($n = 2$) and pityriasis alba ($n = 1$) (S1 Table). A total of 12 samples per group was estimated to be sufficient to attain a power of 85% based on the Welch t-test (PB vs. ODD, MB vs. ODD) with alpha set at 0.03 to replicate the standardized effect size (\log_2FC/SD) estimated from RNA sequencing. Relative expression using the new sample set by RT-qPCR is shown in Fig 2A. Indeed, the validation data are in agreement with RNA sequencing, because 11 tested genes were replicated by RT-qPCR in terms of difference between mean expression (effect size in \log_2FC), except for *STAP1*, *GBP3*, *APOL3* and *CCR7* in PB vs. ODD comparison and *CCR7* in MB vs. ODD (Fig 2B, 2C and S5 Table). As for differentiating leprosy *per se* vs. ODD, genes *IDO1*, *BLK* (exon 11), *CD38*, *CXCL11*, and *SLAMF7*, all had an area under the curve (AUC) of at least 96% with their lower bound 97% confidence intervals above 90% (Figs 2A, 3C and S6 Table).

Next, hierarchical clustering with RT-qPCR data including missing values for some genes (no target gene amplification by RT-qPCR) was performed to examine all samples simultaneously. The analysis roughly revealed three major clusters (Fig 3A). At the highest tree subdivision, one small cluster ($n = 6$) with the dendrogram grouped in light brown was composed of ODD samples with lower expression levels (Fig 3A). Due to several ODD having missing values, we confirmed that these samples had similar gene expression for the reference genes, thereby eliminating the possibility of insufficient cDNA input. Another cluster, grouped in the light purple dendrogram, included all MB and most PB samples (except four in light yellow dendrogram). GA samples displayed two patterns, the first with two samples showing

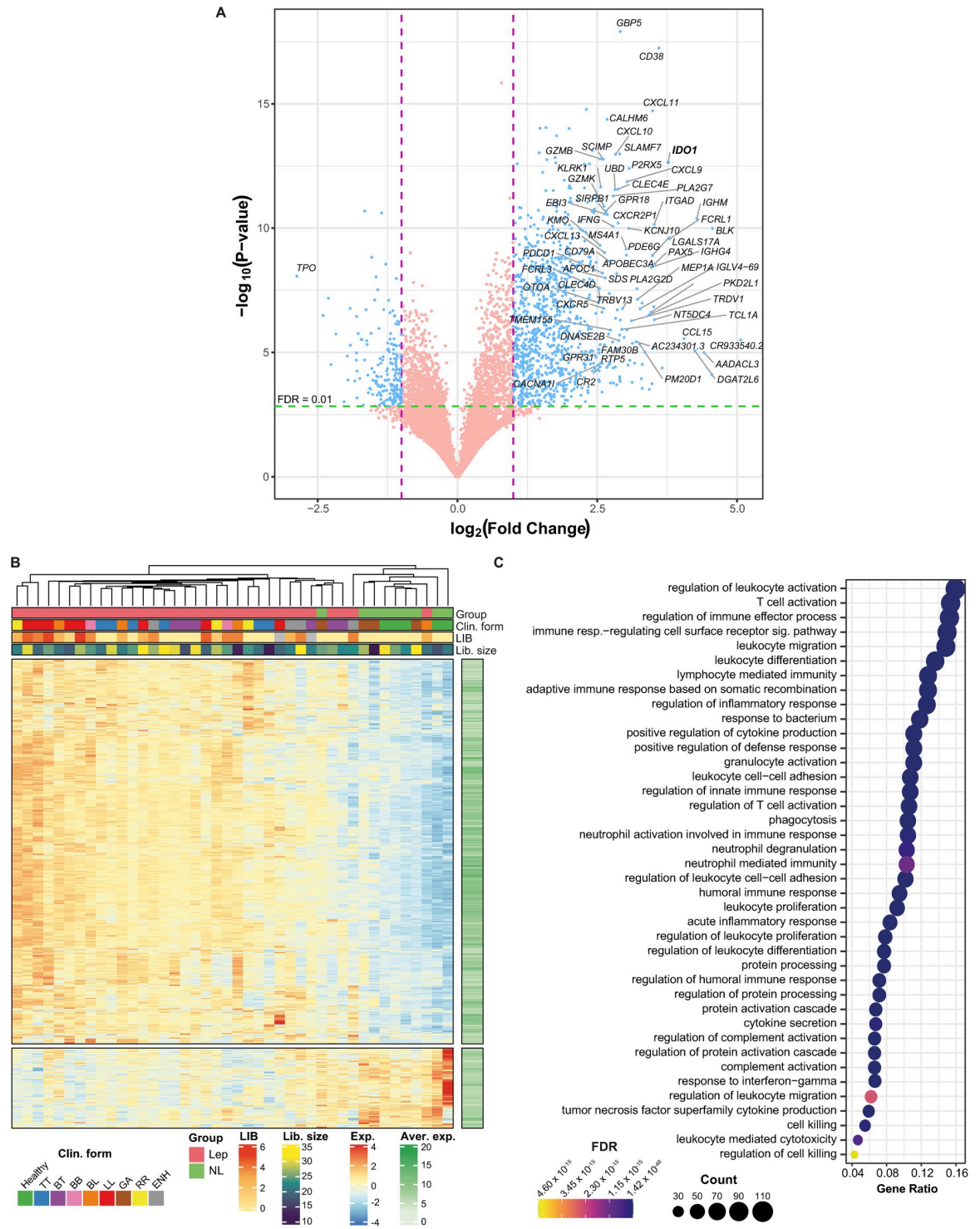


Fig 1. Differentially expressed genes from RNA-seq in leprosy vs. non-leprosy. (A) Volcano plot depicting DEG from leprosy vs. non-leprosy, where violet dashed line marks $|\log_2FC| = 1$. For clarity, gene symbols are shown only for the largest \log_2FC . (B) Heatmap with hierarchical clustering of samples based on expression of the DEG from leprosy vs. non-leprosy comparison. Color scale ranges from lower expression (blue) to higher expression (red). Library size is given in millions. LIB, logarithmic index of bacilli. (C) Biological processes from GO enriched for up-regulated DEG from leprosy vs. non-leprosy comparison. FDR, false discovery rate; NL, non-leprosy; GA, granuloma annulare; non-leprosy: GA + healthy individuals.

<https://doi.org/10.1371/journal.ppat.1009972.g001>

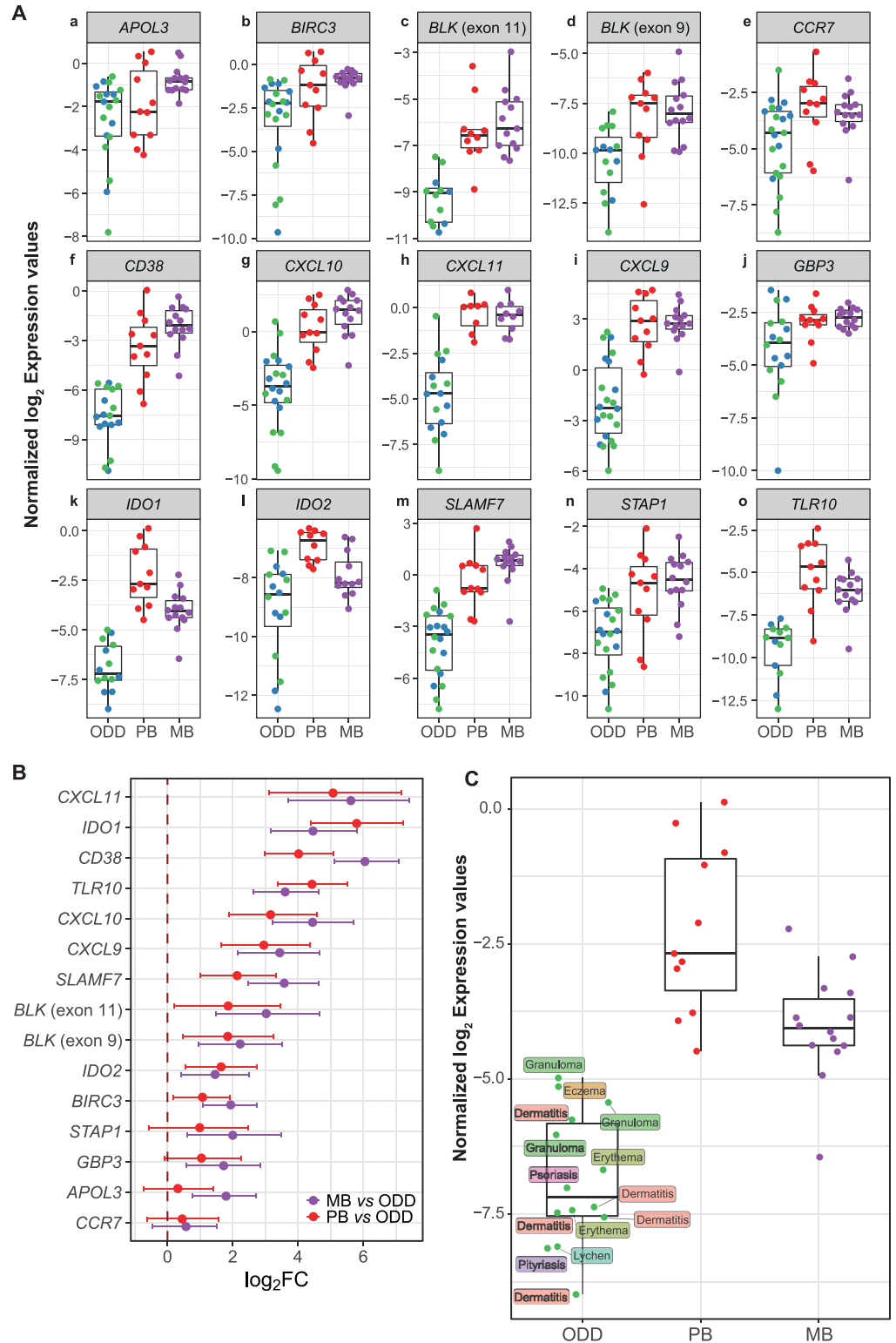


Fig 2. Technical and biological validation for selected DEG discovered from RNA sequencing. (A) Tukey boxplots with RT-qPCR normalized (2–3 reference genes) \log_2 expression values (A.U) according to clinical and histopathological diagnosis. ODD samples are colored according to *M. leprae* 16S rRNA qPCR status as positive (blue) or negative (green). (B) \log_2FC from MB-ODD and PB-ODD comparisons estimated from Bayesian linear mixed models and their 95% credible intervals. (C) Tukey boxplot highlighting *IDO1* RT-qPCR normalized \log_2 expression values by final diagnosis grouped into ODD category. Missing values are omitted.

<https://doi.org/10.1371/journal.ppat.1009972.g002>

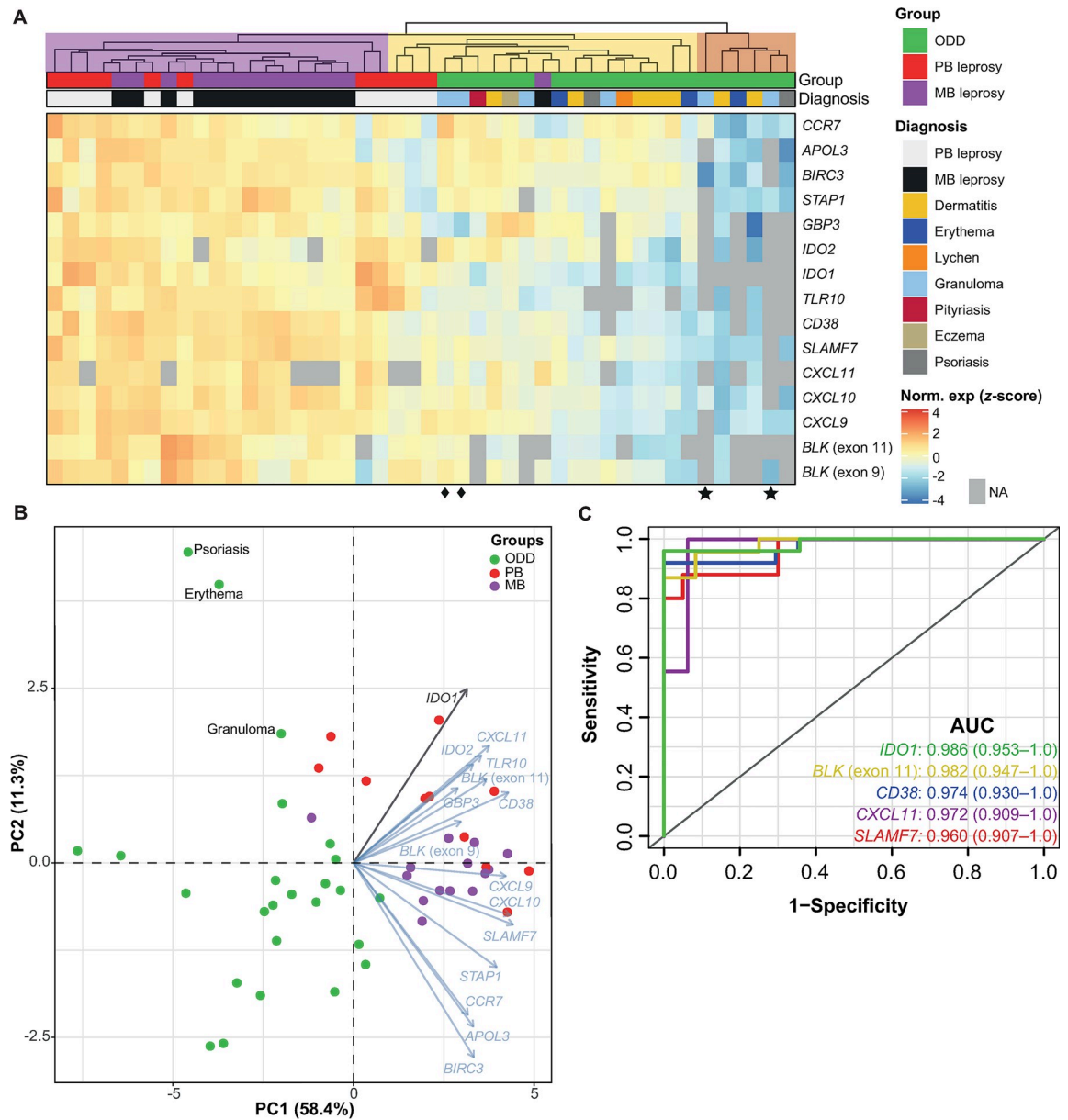


Fig 3. Hierarchical clustering of RT-qPCR replicated DEG and ROC analysis. (A) Hierarchical clustering with scaled and centered normalized \log_2 RT-qPCR expression values (arbitrary units) and annotated according to group and specific diagnosis. Dendrogram tree was cut arbitrarily and cluster analysis is for hypothesis generating purposes only. Two samples had more than 13 missing expression values and were removed from A. (B) Principal component analysis (PCA) with 15 genes measured by RT-qPCR and using \log_2 normalized scaled data. For PCA only, missing values were imputed by the gene arithmetic mean. NA, not amplified, i.e., $C_p > 40$. In this regard, there were two outliers (psoriasis and erythema), which are samples with high numbers of NA values and that were imputed using the gene arithmetic mean. (C) Receiver operating characteristic analysis for genes with largest AUC (97% confidence intervals) from RT-qPCR replication samples (complete data are shown in S6 Table). See also S1 Appendix.

<https://doi.org/10.1371/journal.ppat.1009972.g003>

undetectable *IDO1* expression (Fig 3A, bottom star symbols). The second set ($n = 4$) is scattered among other ODD samples (Fig 3A). It can be seen that GA and PB samples show highly similar expression profiles for some genes (Fig 3A bottom diamond symbols), reinforcing the difficulty in clinically discriminating between these two conditions, and underlining the relevance of their inclusion in our comparisons [29–31].

Then, by applying principal component analysis (PCA) to the 15 gene signature obtained with the expanded sample panel tested by RT-qPCR, we uncovered two major patterns separating leprosy lesions from ODD (Fig 3B). As expected, MB samples appeared more homogeneous than PB and ODD samples, while the latter were more dispersed revealing heterogeneous expression patterns (Fig 3B).

Next, we quantified the individual classification potential of these genes in distinguishing leprosy from ODD using ROC analysis on RT-qPCR data. *IDO1* expression alone was found to be 98% accurate using an arbitrary threshold, followed by *BLK* (exon 11), *CD38*, *CXCL11*, and *SLAMF7* (Fig 3C and S6 Table). Finally, to confirm the causal link between mycobacteria and our gene-set, we evaluated the mRNA profiles induced by other live-mycobacteria using a public RNA-seq dataset [32]. We observed that most gene expression signatures, including *IDO1*, could be successfully replicated as induced by either *M. leprae* and/or other mycobacteria (S1 Appendix and S7 Table). By contrast, some of the tested genes such as *BLK*, *CXCL9*, *MS4A1*, and *TLR10* were not differentially expressed in any of the *in vitro* assays with mycobacteria (S1 Appendix and S7 Table).

MB and PB gene expression profiling and mRNA-based classifier

To define a small subset of genes with high classificatory potential (i.e. with non-overlapping expression values) to distinguish MB from PB lesions, we performed a penalized logistic regression (LASSO) model with k-fold cross-validation trained on the public microarray dataset [24]. This dataset was chosen because of the higher number of PB/MB samples compared to our RNA-seq dataset. As a result, three genes with non-zero coefficients were selected by the cross-validated LASSO model: *HS3ST2*, *CD40LG*, and *CCR6*, but only the first two genes were most frequently (~80%) selected across 10,000 bootstrapped samples within the training dataset (Fig 4A and 4B). The median misclassification error estimated by the resampling was about 4% ($\pm 5.4\%$ median absolute deviation), ranging from 0% to 32% (Fig 4C). Instability assessment in the number of selected genes by LASSO (Fig 4D) showed that most iterations resulted in four non-zero genes (range, 1–20). The final model containing the three genes (*HS3ST2*, *CD40LG*, and *CCR6*) was evaluated on two test RNA-seq datasets: our dataset and the one from Montoya *et al.* including MB (n = 9) and PB (n = 6) groups [28]. Penalized logistic regression demonstrated an accuracy of 100% (lower 95% CIs: 86.8% and 78.2%, respectively) in classifying MB from PB samples in both test RNA-seq datasets; yet, the Brier score indicated a better performance in Montoya's *et al.* dataset, probably due to a more homogeneous sampling (Fig 4E and 4F). The *HS3ST2* gene was consistently more expressed in MB leprosy lesions compared to PB, whereas the opposite was observed for *CD40LG* (Fig 4E and 4H) and *CCR6* (S1 Fig). In both datasets, the combined expression levels of *HS3ST2* and *CD40LG* showed good discrimination between the two groups (Fig 4E and 4H). However, given the sample size and the bootstrapped estimates, it is not currently possible to exclude *CCR6* from the model without additional replication.

Next, to assess the dichotomy beyond cellular *vs.* humoral response in leprosy lesions [33,34], a comparison of gene expression in MB leprosy (LL+BL+BB) *vs.* PB (TT+BT) skin lesions was performed. Differential expression analysis with $|\log_2FC| \geq 1$ and $FDR \leq 0.01$ resulted in 112 DEGs; 69 up-regulated and 43 down-regulated (Fig 5A and S8 Table). In addition, we compared DEG to the public microarray data available in Gene Expression Omnibus (GEO) from Belone *et al.* [24,35] using only the FDR cutoff. With an $FDR < 0.01$, 161 DEGs were common to both studies, all except one showed concordant modulation characterized by an overall high correlation coefficient and concordance index, irrespective of the technology used, the sample processing, and the data analysis methods (Fig 5B).

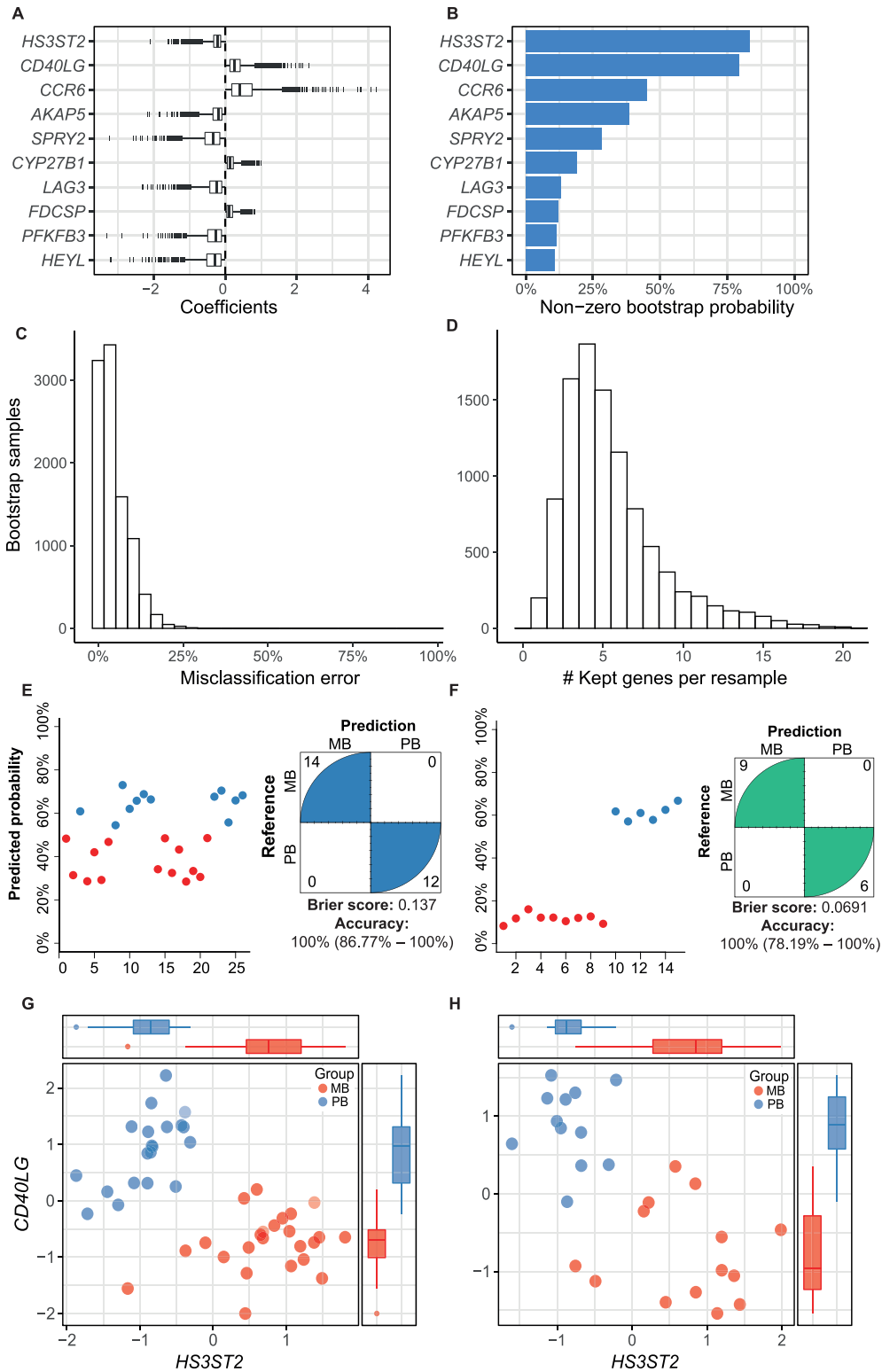


Fig 4. Gene candidates identified with the penalized logistic regression (LASSO) model as the most important to distinguish PB and MB leprosy lesions. (A) Coefficients (log odds) from the top 10 most selected genes (i.e., non-zero) across 10,000 bootstrap samples using the microarray from Belone *et al.* as training dataset. (B) Frequency of non-zero coefficients across all bootstrap samples. (C) Misclassification error distribution estimated from 4-fold cross-validation (k-) across 10,000 bootstrap samples, with median error of 3.70% ($\pm 5.4\%$ median absolute deviation). (D) Number of genes kept across all resamples. Predicted probability from the final model performance on this study test RNA-seq (E) and Montoya

et al. RNA-seq (F). Normalized \log_2 gene expression (z-score) of the two most frequently selected variables for distinguishing MB from PB samples in the (G) microarray training dataset and (H) this study test RNA-seq. PB, paucibacillary leprosy; MB, multibacillary leprosy. Tukey box plots with 1st, 2nd and 3rd quartiles $\pm 1.5 \times$ inter quartile range (IQR) whiskers. See also [S1 Fig](#).

<https://doi.org/10.1371/journal.ppat.1009972.g004>

Functional enrichment analysis of the RNA-seq up-regulated genes (i.e., more expressed in MB than PB) revealed processes involved with regulation of immune response, humoral immunity, phagocytosis, cholesterol metabolism, complement activation among others ([Fig 5C](#) and [S9 Table](#)). On the contrary, enrichment analysis of genes more expressed in PB revealed biological processes such as leukocyte differentiation, lymphocyte differentiation, lymphocyte-mediated immunity, B cell activation, STAT cascade activation/regulation, and JAK-STAT cascade activation ([Fig 5D](#) and [S10 Table](#)), which are consistent with exacerbated responses in granulomatous diseases. Localized clinical forms, i.e., BT and TT, show a gene expression pattern indicative of differentiation towards epithelioid transformation and granuloma assembly, which is also observed in cutaneous or pulmonary sarcoidosis [[36,37](#)].

Epithelial-mesenchymal transition (EMT) in the skin of multibacillary leprosy patients

To make the most of our dataset, we sought to test a previous hypothesis generated from our group's microarray meta-analysis results, in which we have identified a consistent down-regulation of cornification, keratinocyte differentiation, and epidermal development-related genes in leprosy lesions, predominantly in MB [[35](#)]. We first hypothesized that such regulation could result from *M. leprae* inducing dedifferentiation of keratinocytes, similar to the phenomenon described previously in infected Schwann cells [[38](#)], and also seen in skin cancer by a process known as epithelial-mesenchymal transition (EMT) [[39,40](#)]. To test the hypothesis that such modulation was involved with EMT, we correlated the expression of the previously identified down-regulated genes in leprosy [[35](#)] with a collection of genes involved with previously Schwann cell dedifferentiation by *M. leprae* (Masaki *et al.* [[38](#)] signatures for EMT and non-EMT genes), positive markers of EMT (from literature), as well as annotated EMT and mesenchymal-related genes from Reactome (R.HSA.452723, R.HSA.5619507.3, R.HSA.2173791) and Gene Ontology (GO0001837) databases. Briefly, the normalized \log_2 expression matrices were filtered to retain only genes of interest. Then, the pairwise expression correlation for all genes was calculated using the Spearman's rank correlation procedure. Finally, after adjusting the P-values for multiple testing, the genes with any pairwise correlation passing $FDR \leq 1 \times 10^{-4}$ and $\rho \leq -0.8$ were visualized using a heat plot. As result, with this study's RNA-seq, we found a consistent moderate negative correlation between keratinization, cornification, and epidermal development genes ([Fig 6A](#), blue stars, *AQP3*, *DMKN*, *DSG1*, *DSP*, *EFNB2*, *JAG1*, *JAG2*, *KRT5*, *KRT10*, *KRT15*, *KRT19*, *OVOL2*, *PKP1*, *TACSTD2*) with those involved with canonical/alternative EMT and mesenchymal phenotypes ([Fig 6A](#), green stars, *CTSZ*, *MMP9*, *PSAP*, *RHOA*, *TGFBR1*, *TGIF2*, *ZEB2*, *TGFB1*). Interestingly, the strongest correlations with epidermal/keratinocyte genes was with TGF β -EMT-related genes ([Fig 6A](#) blue block), as opposed to Masaki *et al.* non-EMT and other mesenchymal/pluripotency pathways. Next, we replicated these observations with Belone *et al.* microarray [[24](#)] and Montoya *et al.* RNA-seq datasets [[28](#)], respectively. In [Fig 6B](#) and [6C](#) the strongest and representative correlations from TGF β -EMT-related pathway and a keratinocyte/epidermal gene signature are shown in detail, while the remaining are available in [S2](#) and [S3](#) Figs.

Overall, these results showed a decreased expression pattern of EMT-related genes in healthy skin samples, and a linear expression increase in PB and MB patients, especially with

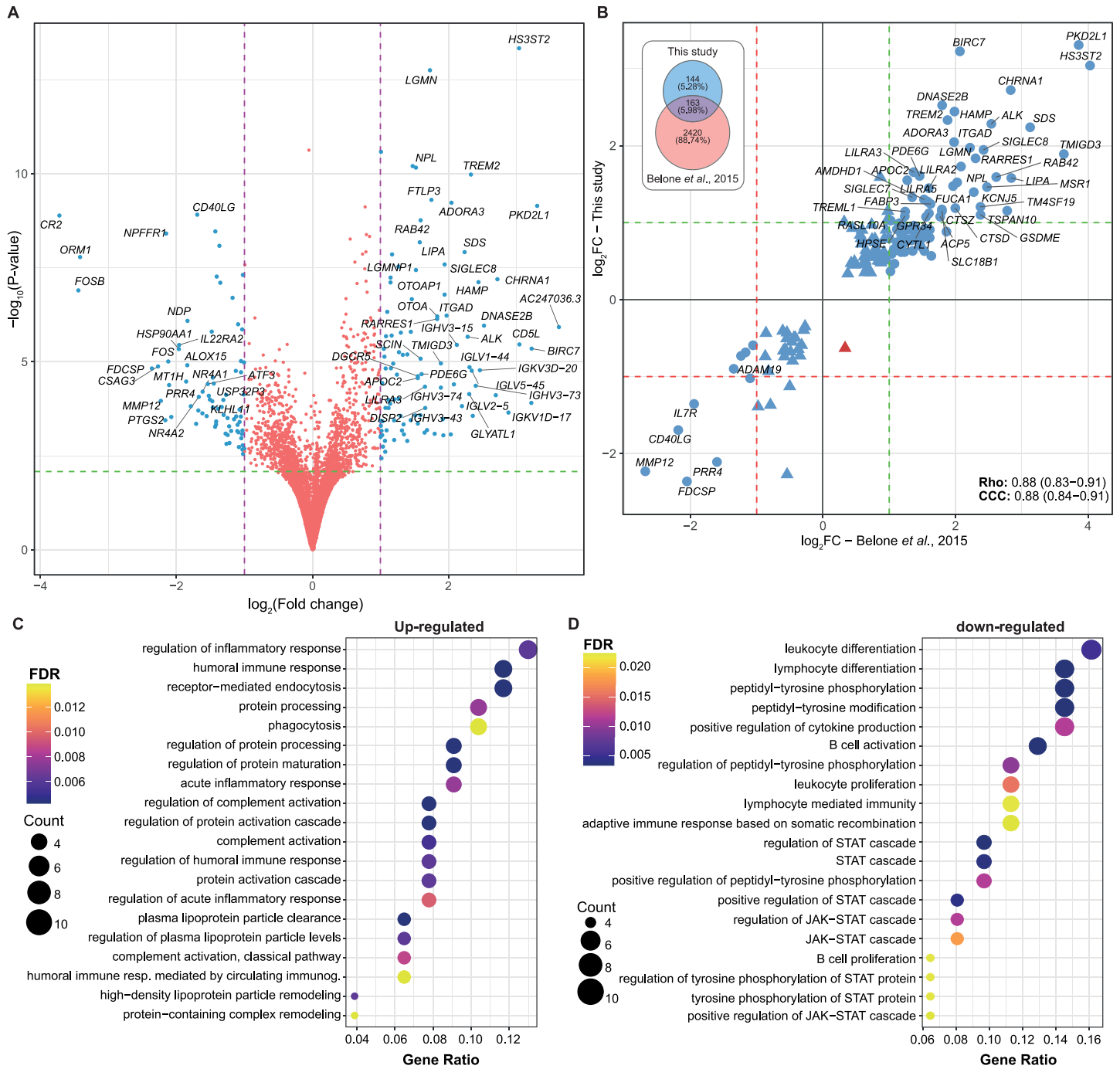


Fig 5. Differentially expressed genes from multibacillary (MB) vs. paucibacillary (PB) leprosy lesions. (A) Volcano plot showing DEG from the MB vs. PB comparison, where blue points are DE with $|\log_2FC| \geq 1$ and $FDR < 0.1$. (B) Scatter plots with the 161 DEG common between this study and Belone *et al.* (24) microarray for the same comparison. Red and green dashed lines indicate \log_2FC of -1 and 1, respectively. Blue points are genes with the same modulation signal and red indicates discordancy. Rho, Spearman's rank correlation coefficient. CCC, Lin's concordance correlation coefficient. Venn diagram on the right displays the number of DEG in each study according to $FDR < 0.01$. (C) Biological processes from GO enriched from up-regulated and (D) down-regulated DEG. FDR, false discovery rate.

<https://doi.org/10.1371/journal.ppat.1009972.g005>

the microarray dataset, except for *MMP9* (Fig 6C). This was accompanied by the previously reduced expression of cytokeratins and epidermal development genes observed in leprosy. From these results, we hypothesize that in addition to $TGF\beta$ -dependent immunosuppression in MB

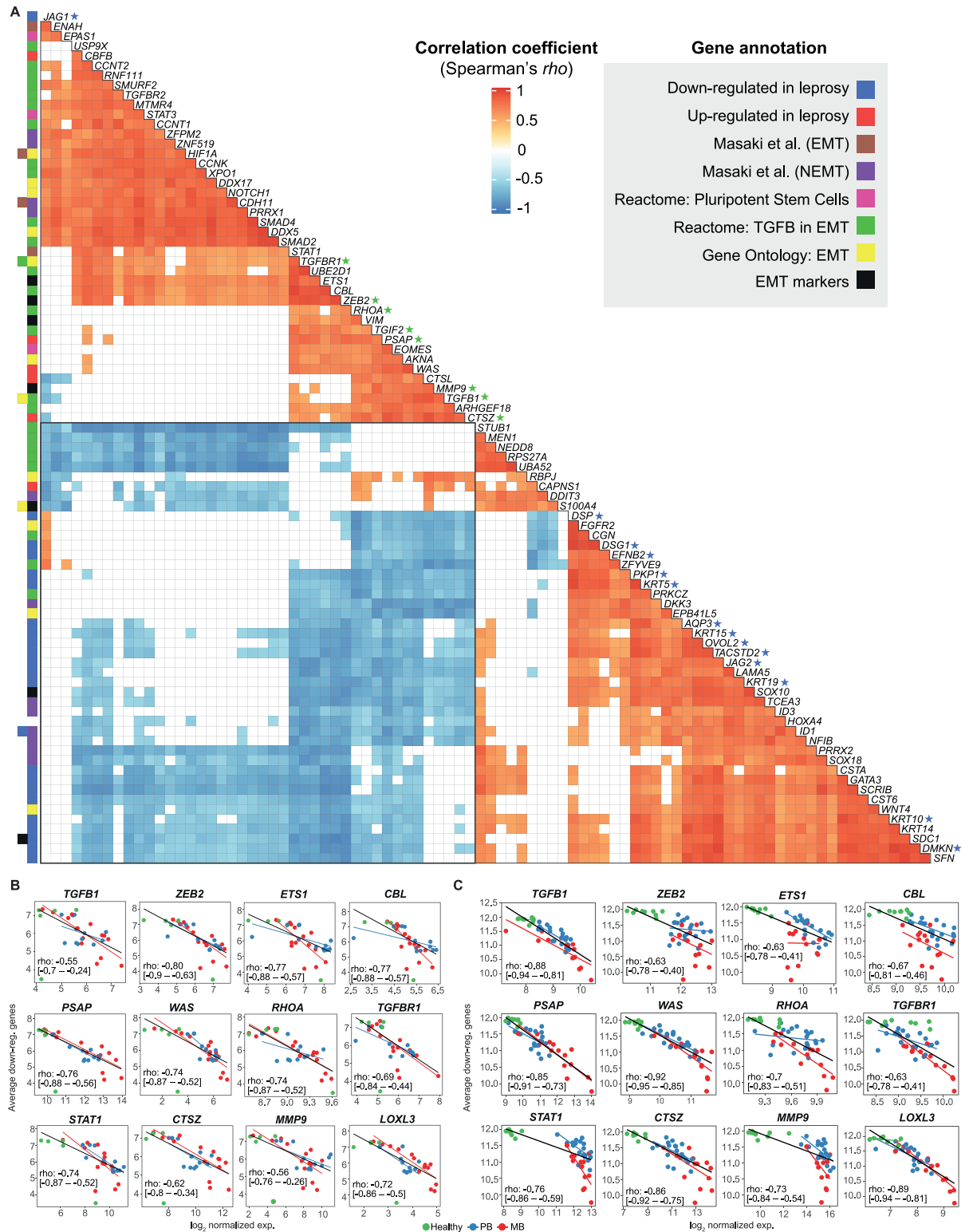


Fig 6. Strongest correlations between keratinocyte and EMT-related genes in leprosy lesions. (A) Heat plot with Spearman's ρ correlation coefficient of the strongest correlations after multiple testing adjustment with at least one gene-pair showing $FDR \leq 0.0001$ and $\rho \leq -0.8$. Correlations with $FDR > 0.1$ are filled with white. Row colored squares identify gene annotations. Scatter plots of average log₂ expression calculated with keratinocyte/epidermal development-related genes previously documented as down-regulated in leprosy skin against dedifferentiation-related genes using either (B) this study RNA-seq dataset or (C) Belone *et al.* microarray (GSE74481). Lines were

drawn based on intercept and beta parameters estimated from robust linear regression for all samples (black line) or separately for PB (blue line), and MB (red line). Spearman's ρ coefficient along with 95% nominal confidence intervals are shown inside scatter plots calculated from all samples. See also S2 and S3 Figs.

<https://doi.org/10.1371/journal.ppat.1009972.g006>

patients, activation of this pathway could be slowing or arresting keratinocyte cornification processes in leprosy lesions thereby both facilitating survival and/or spread of *M. leprae*. If not involved with dedifferentiation of keratinocytes or other epithelial cells, an alternative explanation would be loss of epithelial barrier in MB patients, possibly enlightening a new *M. leprae* transmission route. Further mechanistic experiments ought to determine the causality of our observations and test these findings in light of our hypothetical explanations of the phenomenon.

Discussion

One of the priorities in leprosy research is the development of reliable and accurate laboratory diagnosis tools for all leprosy forms to provide efficient treatment and prevent disability [41]. This goal includes diagnosing patients with early forms of the disease, those with low or mild apparent symptoms, thus assisting with ambiguous differential diagnoses, and even classifying the disease for treatment (MB vs. PB) [4].

Host response to infection as measured by gene expression in skin biopsies offers diagnostic, prognostic and predictive potential. By applying host transcriptomics to skin lesions from leprosy patients and other common confounding dermatoses that challenge clinicians and pathologists [9,30], we identified a small set of genes that provide a promising expression signature capable of distinguishing PB leprosy cases from other confounding dermatological diseases. The top candidate, *IDO1*, is a gene involved in nutritional immunity and metabolism [42–45]. Alone, the expression of this gene was able to differentiate leprosy from non-leprosy lesions with high accuracy in our dataset and in others. According to the latest data from single-cell analysis [46], *IDO1* has been shown to be differentially expressed in Langerhans cells from leprosy lesions compared to healthy skin, corroborating our findings. However, *IDO1* expression is also increased in other mycobacterial diseases such as tuberculosis [47,48], which might decrease its specificity. The accuracy of classification could be improved by combining measurement of *IDO1* expression with that of four other biomarker genes *BLK*, *CXCL11*, *CD38*, *TLR10* and *SLAMF7*, which also showed high classification accuracy in the replication dataset. In parallel, the penalized logistic regression model, evaluated on two independent datasets, demonstrated that *HS3ST2* and *CD40LG* hold potential to differentiate between MB and PB lesions. In parallel, the penalized logistic regression model, evaluated on two independent datasets, demonstrated that *HS3ST2* and *CD40LG* hold potential to differentiate between MB and PB lesions. We recognize that there is no clinical utility in classifying MB from PB lesions with laboratory assays because this can be done during anamnesis alone. Hence, we aimed at identifying molecular features differing not only in the measure of effect (\log_2FC) but also having little overlap between the lesion types, as this may point to previously unexplored genes and pathways relevant to future investigation. Considering the functional evidence for *HS3ST2* [49], it is possible that this gene may be involved with granuloma disassembly, tissue permeability, and cellular migration in leprosy, which would explain its overexpression in MB lesions. On the contrary, *CD40LG* (also known as CD154) is more expressed in PB patients when compared to MB with a predominant role in the activation of the microbicidal *Th1* response associated with PB lesions [50]. After mechanistic validation of our findings, quantifying expression levels of *HS3ST2* and *CD40LG* from leprosy lesions could be useful to assess immune responsiveness against *M. leprae*, help patient stratification and/or provide a basis for host-based adjuvant treatment for leprosy lesions.

One of the challenges in translating gene expression signatures into medical diagnosis is the cost of measuring a large number of genes and transforming these values into a unique continuous or binary classifier. So far, we were able to reproduce the findings using both bulk RNA-sequencing and relative RT-qPCR, with the latter being more accessible to clinicians at least in reference centers or central hospitals. Although there are successful approved RT-qPCR relative gene expression-based diagnostic tests for diagnosing sepsis [12], clinical support for prostate [22], and breast cancer [18], there is a need for alternatives to reduce the cost and complexity of such assays. Quantification of mRNA based on isothermal amplification either with NASBA [51,52], RT-LAMP [53,54] or CRISPR-Cas12 [55] is conceivable for less specialized settings without high-end equipment. Besides, combining a multi-target expression-based diagnostic test with qPCR detection of *M. leprae* DNA could increase the specificity and sensitivity of leprosy diagnosis [56]. Alternatively, an ELISA assay measuring the levels of IDO1 protein from skin interstitial fluid, for example, could be proven useful [57]. Further studies ought to be done selecting tangible diagnostic thresholds and devising a proper classification system to allow the biomarker to function unsupervised.

In parallel with poor diagnosis, lack of fundamental understanding of leprosy pathogenesis has misled scientists for centuries [5,6]. Herein, we also compared the two leprosy poles, MB and PB, and identified several pathways already known to be associated with leprosy, such as the humoral immune response, phagocytosis, and complement activation. Genes involved with cholesterol and fatty acids were more expressed in MB lesions, as already reported [58–60]. Interestingly, B-cell-related genes were more expressed in PB than MB. In fact, it seems that both poles modulate this pathway by a distinct set of genes. Involvement of B lymphocytes in PB leprosy pathogenesis has been described by a few groups, which may indicate differential involvement of such cells depending on the disease pole [61,62].

M. leprae subverts host cell metabolism [63] by inducing lipid biosynthesis, while avoiding type II (IFN- γ) responses through a type I IFNs mechanism, following the phagolysosomal breach that releases DNA into the cytosol [64]. However, exactly how the bacilli spread throughout the body and bypass the microbicidal immune response remains unknown. Here, we provide robust evidence indicating that *M. leprae* may induce EMT in the skin within keratinocytes and macrophages, as described in Schwann cells [38]. Indeed, *M. leprae* induced dedifferentiation of infected Schwann cells into an immature stage resembling progenitor/stem-like phenotype [38]. These reprogramming events induced by long-term infection with *M. leprae* resulted in mesenchymal cells capable of migratory and immune-permissive behavior, which in turn facilitated *M. leprae* spread to skeletal and smooth muscles and furthered macrophage recruitment [38,65]. In our previous work, we identified a down-regulated signature of keratinocyte differentiation and cornification gene markers in MB skin lesions [35]. Here, we showed that such genes are inversely correlated with genes involved with EMT, especially the members of the TGF β -EMT pathway, such as *TGFB1*, *TGFBRI*, *TGIF2*, *PSAP*, *ZEB2* [66,67]. Some of these genes are directly or indirectly associated with EMT, such as a *PSAP* [68], *WAS* [69], *RHOA* [70–73], *CTSZ* [74], *MMP9* [75], *LOXL3* [76], *HIF1A* [77,78] among others.

Our hypothesis that *M. leprae* is inducing dedifferentiation or slowing the cornification process in keratinocytes is plausible, given the evidence in Schwann cells and a few reports of infection in this cell type (Fig 7) [79,80]. Nevertheless, other phenomena could explain EMT's role in leprosy pathogenesis, such as wound healing or loss of the epithelial barrier. Although, given its obligatory intracellular lifestyle, *M. leprae* induces dedifferentiation in other cell types, either directly as in Schwann cells or indirectly via chemokine and cytokine production in lesions. Besides inducing keratinocyte dedifferentiation to mesenchymal cells, *M. leprae* might benefit from a decreased or alternative immune activation of these cells [81,82]. Further

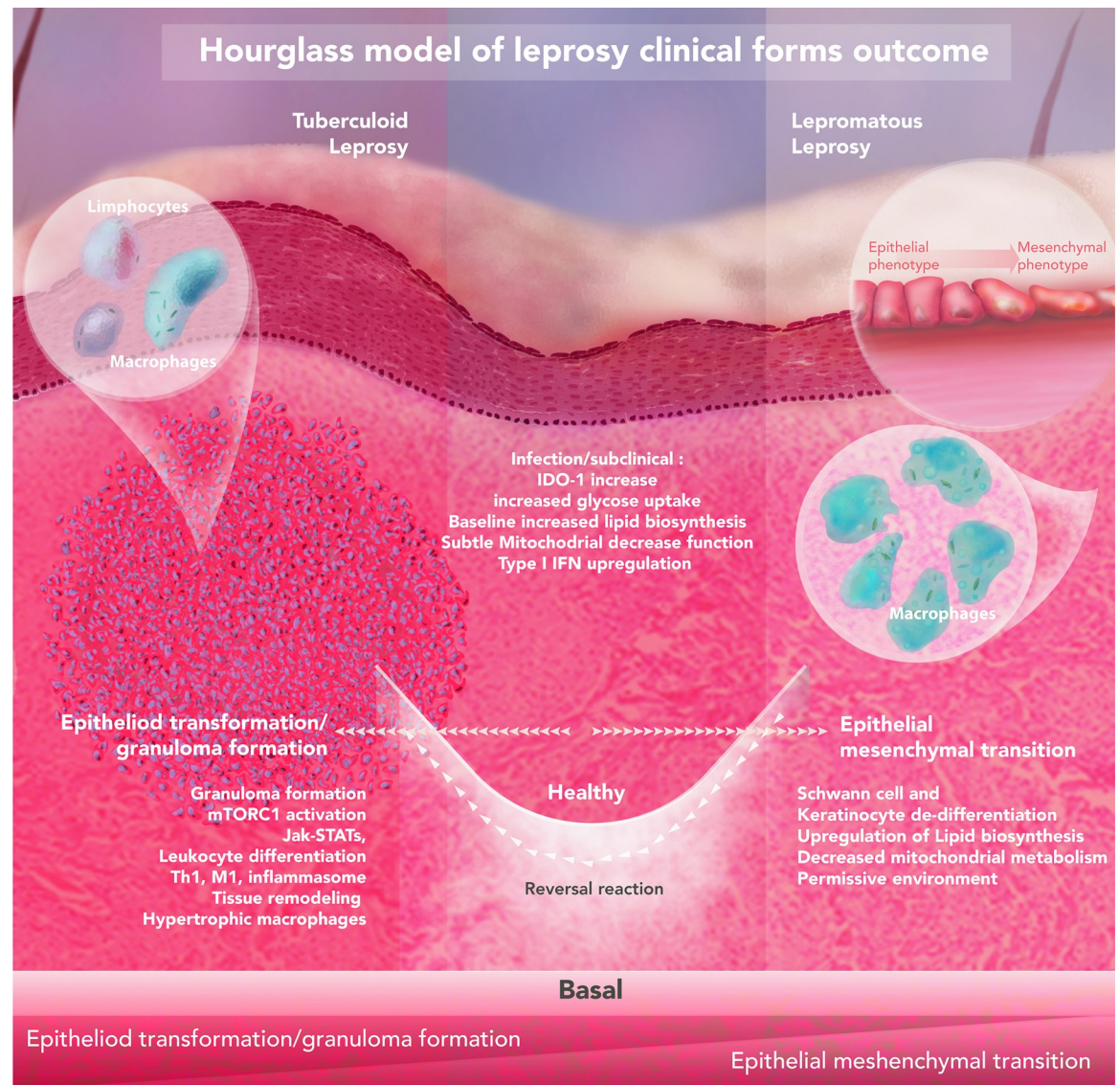


Fig 7. Hypothetical hourglass model contextualizing the observed findings for leprosy clinical outcomes. The host-pathogen interaction in the skin leads to opposing leprosy clinical forms. Upon infection, *M. leprae* induces baseline metabolic alterations such as an increase in glucose uptake, modulation of lipid biosynthesis, reduction of mitochondrial metabolism, and upregulation of IDO-1 and type I IFN. Eventually, progression towards an unspecified inflammatory state can be observed where three ways could be anticipated: I) self-healing; II) progression towards the tuberculoid pole; or III) progression to lepromatous pole. These outcomes are driven by specific environmental and host genetic factors. It is expected that lower (or shorter) *M. leprae* exposure, food shortage, BCG vaccination, and polymorphisms in genes controlling autophagy/granuloma formation (*NOD2*, *LRRK2*, *PRKN*) all contribute to developing leprosy per se. Excessive inflammation is one phenotype observed, that is also seen in other granulomatous diseases (e.g., cutaneous sarcoidosis, granuloma annulare), especially in paucibacillary lesions. On the other pole, epithelial-mesenchymal transition and local immunosuppression are present due to a probably higher (and/or longer) *M. leprae* exposure, combined with host single-nucleotide polymorphisms (SNPs) at key genes, like lipid biogenesis (*APOE*) and central metabolism (*HIF1A*, *LACCI/FAMIN*), culminating in disease progression.

<https://doi.org/10.1371/journal.ppat.1009972.g007>

functional confirmatory experiments should elucidate the causality of this correlation and provide definitive evidence of the relationship between the bacilli and other cell types, such as keratinocytes, fibroblasts, and epithelial cells.

Our preliminary data also showed that the enriched pathways among PB skin lesions were consistent with profiles observed in other granulomatous diseases, such as noninfectious sarcoidosis and granuloma annulare, or chronic infectious diseases like tuberculosis [37,83–85]. Our findings revealed that PB (TT/BT) lesions have, among others, JAK-STAT cascade activation, which has been implicated in sarcoidosis and GA. Remarkably, the JAK-STAT specific biological inhibitor, tofacitinib, has a potent effect promoting rebalance of exacerbated immunity among sarcoidosis and granuloma annulare patients reestablishing homeostasis [83]. Another compound, everolimus, has been shown in experimental models to achieve the same response [37] suggesting that these drugs could be useful to treat PB, but not MB, leprosy.

To conclude, our combined findings provide highly discriminatory mRNA signatures from skin lesions that could distinguish leprosy from other dermatological diseases and allow disease classification by monitoring only a handful of genes. In addition, we report new genes and pathways that are likely informative regarding how *M. leprae* interacts with and subverts host cells to promote its spread within the body and subsequent transmission.

Materials and methods

Ethics statement

All patients were enrolled after informed written consent was obtained with approval from the Ethics Committee of the Oswaldo Cruz Foundation, number 151/01.

Patient cohort

Leprosy clinical forms were classified according to the criteria of Ridley and Jopling [2]. Leprosy patients were treated according to the operational criteria established by the World Health Organization [4]. Leprosy and patients with other dermatological diseases were eligible if their diagnosis was confirmed by clinical and histopathological findings. Additionally, detection of *M. leprae* DNA by qPCR routinely performed in our laboratory could be employed to support diagnosis [56,86]. HIV and hepatitis B positive patients were not included in this study, in addition, we excluded individuals with a current or previous history of tuberculosis. No other comorbidities were used to exclude patients and further individual information is available in [S1 Table](#). Skin biopsy specimens containing both epidermis and dermis were obtained with 3 mm (diameter) sterile punches following local anesthesia from the lesion site. Skin biopsies were immediately stored in one milliliter of RNALater (Ambion, Thermo Fisher Scientific Inc., MA, USA) according to the manufacturer's instructions and stored in liquid nitrogen until RNA isolation. Healthy skin biopsies were from lesion-free sites of patients diagnosed with indeterminate or pure neural leprosy.

Study design

The main objective of this research was to identify host gene expression patterns capable of distinguishing leprosy (including the PB forms) from other differential diagnosis of skin lesions. Our working hypothesis was that leprosy lesions, despite their morphological and histopathological similarity to other skin diseases, may induce distinct patterns of gene expression in a small subset. We predefined the comparison of leprosy (PB+MB) from non-leprosy including GA in addition to healthy patients for RNA sequencing experiment. In addition, we predetermined comparisons between leprosy poles: MB vs. PB. Our samples are representative of a population of individuals attending the Sousa Araujo Outpatient Clinic based in Rio de Janeiro, Brazil, which also receives patients from surrounding municipalities.

RNA isolation

Snap frozen skin biopsies were thawed in wet ice and processed using TRIzol Reagent (Ambion, Thermo Fisher Scientific Inc., MA, USA) according to the manufacturer's instructions with the help of Polytron Homogenizer PT3100 (Kinematica AG, Switzerland). RNA was treated with DNase using the DNafree kit (Thermo Fisher Scientific Inc., MA, USA) according to the standard manufacturer's protocol, prior to use for library preparation and RT-qPCR. RNA integrity was assessed in 1% agarose gel electrophoresis or TapeStation RNA ScreenTape (Agilent Technology, CA, USA). During RNA isolation, samples were randomly assigned to extraction batches and freeze-thaw cycles to minimize batch effects and the introduction of technical artifacts. All procedures applied to samples were carried out using reagents from the same lot. The first author conducted the experiments aware of each sample group during the entire process, therefore, no blinding scheme was used, although we do not rely on perceptual/abstract measurements or analyses nor did we purposefully exclude samples.

Library preparation and Illumina RNA sequencing

RNA-seq libraries were prepared with 1 µg of total RNA for each sample using the Illumina TruSeq mRNA kit (Illumina, USA) as recommended by the manufacturer using the Illumina CD RNA indexes (Illumina, USA). Libraries were quantified and qualified using a qPCR quantification protocol guide (KAPA Library Quantification Kits for Illumina Sequencing platforms) and TapeStation D1000 ScreenTape (Agilent Technologies, USA), respectively. The resulting libraries (fragment size 200–350bp) were multiplexed (17, 17, and 19 libraries, respectively) and sequenced using the NextSeq 500 platform (Illumina, USA), generating approximately 520 million single-end reads of 75 nucleotides in length.

RNA-sequencing analysis

RAW bcl files were converted into fastq using Illumina's bcl2fastq script. Then, read quality was assessed using FastQC version 0.11.8 [87]. Next, transcript counts were estimated using Salmon (v.1.13.0) quasi-mapping (human transcriptome GRCh38_cdna sourced from Ensembl/RefGenie plus pre-computed salmon index, http://refgenomes.databio.org/#hg38_cdna) with default settings and `—seqBias` flag set [88]. Transcript counts were summarized into ENSEMBL gene counts using the R v.3.6.1 package tximport v.1.12.0 [89,90] and biomaRt v.2.40.5 [91]. The expression of sex-chromosome-specific genes, such as *UTY* and *XIST*, was used to rule out sample mislabeling. Differential expression was estimated using DESeq2 v.1.24.0, after filtering out weakly expressed genes with less than 10 counts per million and less than 15 total counts in 70% of samples [92–94]. In addition to the patient's biological sex, extraction batch and sequencing run, three surrogate variables estimated with RUVseq v.1.18.0 were included in DESeq2's generalized linear model [95,96]. Nominal P-values were inspected with histograms and adjusted for multiple testing according to the method [97] proposed for controlling the false discovery rate (FDR). All log₂ fold-changes were shrunken prior to DE filtering with the `apeglm` [94] or normal algorithms. For visualization, counts per million (CPM) were computed with edgeR's `cpm` function v.3.26.1 and variance stabilized with the parametric method [92]. Then, surrogate variables and covariates were regressed out from the expression matrix using limma's `removeBatchEffect` [98–100] before being visualized with ggplot2 v.3.3.0 [101]. Hierarchical clustering, heatmaps, and ROC analysis were all performed with the previously processed expression matrix. Heatmap with hierarchical clustering was drawn with ComplexHeatmap v.2.0.0 [102] or pheatmap v.1.0.12 [103] using gene-wise scaled and centered matrix with Euclidean distance and average agglomeration method.

Overrepresentation analysis (ORA) was used to test for Gene Ontology Biological Process (GO BP) enrichment with clusterProfiler v.3.12.0 [104] and org.Hs.eg.db v.3.8.2 annotations [105]. Up and down-regulated lists were used as inputs and the background list was composed of all genes subjected to differential expression. P-values were adjusted for multiple testing using the Benjamini-Hochberg method [97]. Raw and normalized RNA sequencing data are available in EMBL-EBI's ENA and ArrayExpress under accessions ERP128243 and E-MTAB-10318, respectively.

RT-qPCR

A total of 2.5 μg of RNA was reversed transcribed into cDNA using 4 μL of Vilo Master Mix (Thermo Fisher Scientific Inc., USA) according to the manufacturer's instructions. Then, cDNA was diluted to a final concentration of 5 $\text{ng}/\mu\text{L}$ using TE buffer (10 mM Tris-HCL and 0.1 mM EDTA in RNase-free water). RT-qPCR was performed using Fast Sybr Master Mix (Thermo Fisher Scientific Inc., USA) in a final reaction volume of 10 μL . For each reaction, performed in duplicate, 5 μL of Fast Sybr Green were combined with 200 nM of each primer, 10 ng of cDNA, and q.s.p of injection-grade water. Thermal cycling and data acquisition were performed on Viiia7 with 384 well block (Applied Biosystems, Thermo Fisher Scientific Inc., USA) following the master mix manufacturer cycling preset with a final melting curve analysis (65°C to 95°C, captured at every 0.5°C). All primers were designed with NCBI Primer-Blast [106–109] to either flank intron(s) or span exon-exon junction(s) to avoid gDNA amplification (S11 Table). Further, primers were quality checked for specificity, dimers and hairpin with MFEPPrimer v.3.0 [110,111] and IDT's oligoAnalyzer (<https://www.idtdna.com/calc/analyser>). Data were exported from QuantStudio software v.1.3 in RDML format, which was imported to LinRegPCR v.2020.0 for RT-qPCR efficiency determination and calculation of the N_0 value [112,113]. Finally, N_0 values were imported to R and normalized using as the denominator the normalization factor (NF) calculated from the geometric mean of at least three reference genes (*RPS16*, *RPL35* and *QRICH1*), which were previously tested for stability [114]. These N_0 normalized values were used for visualization in Fig 2A. For mean difference estimation between groups, RT-qPCR data were analyzed in a Bayesian framework (Markov Chain Monte Carlo sampling, MCMC) using generalized linear mixed effect models under lognormal-Poisson error with MCMC.qpcr v.1.2.4 [115,116]. Per-gene efficiency estimates from LinRegPCR were used in conjunction with C_p (crossing point) calculated in QuantStudio software v.1.3 to generate the counts table. Then, the generalized linear mixed-effect model was fitted using three reference genes (allowing up to 20% between-group variation) with 550,000 iterations, thin = 100, and burn-in of 50,000. The model specification included the sample (factor with 51 levels) as a random effect and the diagnosis group (factor with 3 levels) as a fixed effect. MCMC diagnostics were done by inspecting chain mixing plots and linear mixed model diagnostic plots. Ninety-five percent credible intervals were drawn around the posterior means and MCMC equivalent P-values were also computed.

Reanalysis of public gene expression datasets

Belone and collaborators GSE74481 [24] and de Toledo-Pinto and cols. GSE35423 [64] microarray datasets were reanalyzed as described elsewhere [35]. Blischak and cols. [32] RNA-seq dataset (GSE67427) was reanalyzed from counts per sample file from the author's Bitbucket repository (<https://bitbucket.org/jdblischak/tb-data/src/master/>). Briefly, a normalized \log_2 expression matrix was regressed out for RNA integrity number and extraction batch variables. Then, differences in gene expression (48h post-infection) for specific genes and treatments were tested using a gene-wise linear mixed model with a random intercept per sample

(replicate) followed by Dunnett comparison against a “mock” group using emmeans v.1.5.3. Montoya and collaborators’ dataset was retrieved from GEO (GSE125943) already normalized (DESeq2 median ratio method) and transformed with base 2 logarithm with no further processing [28].

Correlation analyses

For RNA-seq datasets, normalized \log_2 counts-per-million values were used and \log_2 normalized intensities for microarray. Spearman’s rank correlation method was chosen because it is robust against outliers, does not rely on normality assumption, and also identifies monotonic but non-linear relationships. Initially, a list of keratinocyte/cornification/epidermal development genes that were DE in the meta-analysis was assembled [35]. Then, lists of target genes were compiled from results of Masaki *et al.* [38]: EMT and non-EMT; from Reactome: R-HSA-452723 (Transcriptional regulation of pluripotent stem cells), R-HAS-5619507.3 (Activation of HOX genes during differentiation), R-HAS-2173791 (TGF β receptor signaling in EMT); Gene Ontology GO:0001837 (EMT), and literature for EMT canonical markers. Next pairwise Spearman correlation was calculated using the Hmisc’s rcorr function v.4.2–0 for every pair of genes from keratinocyte/epidermal development and EMT gene lists. P-values were adjusted for multiple testing using the BH method for FDR control for all tests [97]. Additionally, 95% nominal confidence intervals were calculated using the Fieller method implemented by correlation R package v.0.5.0 [117,118]. To visualize the results, only genes with at least one pairwise correlation with Spearman’s rho coefficient ≤ -0.8 and FDR ≤ 0.0001 were selected. Additionally, the average \log_2 expression from genes involved with keratinocyte/epidermal development was calculated and used in scatter plots against the expression of the EMT genes. Scatter plots were drawn with ggplot2 v.3.3.3 showing lines from coefficients estimated using default robust regression (MASS::rlm v.7.3–51.4) either for all samples or stratified by group. No outliers were omitted.

Regularized (LASSO) logistic regression classification

Normalized \log_2 expression matrices regressed out for covariates and batches were used as input predictors. The model was trained using the microarray dataset from Belone *et al.* [24] with penalized regression (L1-norm, LASSO) and 4-fold cross-validation (k-fold CV) with the negative binomial log-likelihood link function, glmnet v.4.1 [119–121]. Predictors were standardized to have mean zero and unit variance inside the cv.glmnet function. We opted for L1-norm because it results in a smaller number of genes ($\#features \leq n$) with non-zero coefficients, as compared to elastic-net or ridge regression counterparts. In addition, this model is suitable for high-dimensional data as it combines feature selection during model tuning and training, mitigating the effects of predictors’ collinearity and reducing overfitting. To assess the coefficients’ error, misclassification error rate, feature stability and model size we used non-parametric bootstrap (boot v.1.3.25) with 10,000 samples, with 4-fold cross-validation inside each loop [122,123]. The final LASSO model selected by 4-fold cross-validation contained three non-zero genes. Finally, independent RNA-seq test datasets were used to compute the accuracy of the final model. Alternatively, the whole process was repeated with leave-one-out cross-validation instead of k-fold. The results were practically indistinguishable, especially regarding the feature stability.

Sample sizes

The sample size for RNA sequencing was selected based on previous leprosy work with microarrays, aiming at detecting genes with at least a differential fold-change of two. For RT-qPCR

validation, sample size calculation was performed using the per-gene standardized effect size estimated from the RNA-seq data, aiming at a power of 85% and $\alpha = 0.03$. No samples were discarded after successful data collection (i.e. outliers). In the end, the sample sizes per group for RT-qPCR were: MB = 14, PB = 11, ODD = 23. All RT-qPCR reactions were conducted in duplicate for each biological unit (here, a fragment of a skin biopsy derived from an individual).

RT-qPCR and ROC statistical analyses

Normalized RT-qPCR gene expression data were \log_2 transformed before use in data visualization. Additionally, we checked if the Bayesian results remained consistent using a more common procedure. For this, the mean normalized expression (from N_0) was compared pairwise for the prior stipulated groups using Welch's t-test implemented in R language, using the pre-determined alpha of 0.03. Normality assumption was verified with normal quantile-quantile plots (qqplots, car v. 3.0–2). In cases where quantile-quantile plots showed huge deviation from theoretical normal distribution, the Wilcoxon Rank Sum was used to verify results.

Receiver Operating Curve (ROC) analysis was used to determine the accuracy (measured by the area under the curve, AUC) and its respective best classification threshold, aiming at maximizing AUC with equal importance for sensitivity and specificity. Confidence intervals (95%) for AUC were calculated using the Delong non-parametric method as implemented in pROC v.1.15.3 [124–126].

Supporting information

S1 Appendix. Linking expression profiles to mycobacteria species.

(DOCX)

S1 Fig. Gene expression in MB and PB groups from test and training datasets. Normalized \log_2 expression values per group from (A) this study RNA-seq dataset or (B) Belone *et al.* (GSE74481) [24]. The genes shown were selected in 25%–50% of the LASSO models (Fig 4B) according to the bootstrap. MB, multibacillary leprosy; PB, paucibacillary leprosy; TT, tuberculoid leprosy; BT, borderline-tuberculoid; BB, borderline-borderline; BL, borderline-lepromatous; LL, lepromatous. Each point represents an independent skin biopsy from a patient. Y-axis values are not comparable between panels A and B.

(PDF)

S2 Fig. Strongest correlations between the average expression of genes associated with keratinocyte/cornification against dedifferentiation-related genes using Montoya *et al.* RNA-seq dataset [28]. Scatter plots of scores (average normalized \log_2 expression) calculated from genes with previously documented down-regulation in leprosy skin lesions against dedifferentiation-related genes with Montoya *et al.* RNA-seq dataset (GSE125943) [28]. Lines were drawn based on intercept and beta estimates from robust linear regression for all samples (black) or separately for TL (tuberculoid leprosy, blue), and LL (lepromatous leprosy, red). X-axis shows \log_2 normalized expression values. Spearman's rho are shown along with nominal 95% confidence intervals inside the plots. Most genes shown have $FDR < 0.1$ and $\rho \leq -0.6$. Related to Fig 6.

(PDF)

S3 Fig. Strongest correlations between modulated genes from keratinocyte/cornification and dedifferentiation-related genes using Belone *et al.* microarray dataset (GSE74481) [24]. Heat plot with Spearman's rho correlation coefficient of the strongest correlations from all ontologies screened after multiple testing adjustment (BH-FDR). Most genes shown have

FDR \leq 0.0001 and $\rho \leq$ -0.7. Bottom colored rectangles indicate which category the gene was present (some genes co-occur). Related to [Fig 6](#).
(PDF)

S1 Table. Demographic and clinical metadata from human participants.
(XLS)

S2 Table. Genes differentially expressed from leprosy vs. non-leprosy with $|\log_2FC| \geq 1$ and FDR \leq 0.01.
(XLS)

S3 Table. Over-representation analysis (ORA) for leprosy vs. non-leprosy (up-regulated) differentially expressed genes.
(XLS)

S4 Table. ROC analysis from RNA-seq dataset using leprosy vs. non-leprosy samples.
(XLS)

S5 Table. Posterior \log_2FC estimates, 95% credible intervals and MCMC P-values from PB-OD and MB-OD comparisons.
(XLS)

S6 Table. ROC analysis results using RT-qPCR with the validation dataset (Related to [Fig 3](#)). 95% confidence intervals are shown, except for AUCs of 1.0. The table is sorted from highest to lowest AUC.
(XLS)

S7 Table. \log_2FC estimates, confidence intervals, and Dunnett P-values from distinct mycobacterial stimuli in human macrophages *in vitro*.
(XLS)

S8 Table. Genes differentially expressed from multibacillary paucibacillary leprosy with $|\log_2FC| \geq 1$ and FDR \leq 0.01.
(XLS)

S9 Table. Over-representation analysis (ORA) for MB vs. PB (up-regulated) differentially expressed genes.
(XLS)

S10 Table. Over-representation analysis (ORA) for MB vs. PB (down-regulated) differentially expressed genes.
(XLS)

S11 Table. Oligonucleotide sequences.
(XLS)

Acknowledgments

The authors wish to acknowledge Suelen Justo Moreira (MSc) and Rhana Prata (PhD) for assistance with skin biopsy RNA isolation. Helen Ferreira (MSc), Cristiane Domingues and José Augusto for their technical and logistic support. The Gene Expression Core Facility (GECF) at EPFL, Lausanne, Switzerland, especially Drs. Elisa Cora and Bastien Mangeat for sequencing assistance. All patients and staff (physicians, nurses and technicians) from Sousa Araujo Outpatient clinic at FIOCRUZ, Rio de Janeiro, Brazil.

Author Contributions

Conceptualization: Milton Ozório Moraes.

Data curation: Thyago Leal-Calvo.

Formal analysis: Thyago Leal-Calvo, Milton Ozório Moraes.

Funding acquisition: Stewart Thomas Cole, Milton Ozório Moraes.

Investigation: Thyago Leal-Calvo, Charlotte Avanzi, Mayara Abud Mendes, Philippe Busso.

Methodology: Thyago Leal-Calvo.

Project administration: Stewart Thomas Cole, Milton Ozório Moraes.

Resources: Roberta Olmo Pinheiro, Euzenir Nunes Sarno, Stewart Thomas Cole, Milton Ozório Moraes.

Software: Thyago Leal-Calvo, Andrej Benjak.

Supervision: Charlotte Avanzi, Stewart Thomas Cole, Milton Ozório Moraes.

Validation: Thyago Leal-Calvo.

Visualization: Thyago Leal-Calvo, Milton Ozório Moraes.

Writing – original draft: Thyago Leal-Calvo.

Writing – review & editing: Charlotte Avanzi, Mayara Abud Mendes, Andrej Benjak, Roberta Olmo Pinheiro, Stewart Thomas Cole, Milton Ozório Moraes.

References

1. Britton WJ, Lockwood DN. Leprosy. *The Lancet*. 2004; 363: 1209–1219. [https://doi.org/10.1016/S0140-6736\(04\)15952-7](https://doi.org/10.1016/S0140-6736(04)15952-7)
2. Ridley DS, Jopling WH. Classification of leprosy according to immunity. A five-group system. *Int J Lepr Mycobact Dis Off Organ Int Lepr Assoc*. 1966; 34: 255–73. PMID: [5950347](https://pubmed.ncbi.nlm.nih.gov/5950347/)
3. Scollard DM, Adams LB, Gillis TP, Krahenbuhl JL, Truman W, Williams DL. The Continuing Challenges of Leprosy The Continuing Challenges of Leprosy. *Clin Microbiol Rev*. 2006; 19: 338–381. <https://doi.org/10.1128/CMR.19.2.338-381.2006> PMID: [16614253](https://pubmed.ncbi.nlm.nih.gov/16614253/)
4. WHO. Guidelines for the Diagnosis, Treatment and Prevention of Leprosy. Geneva: World Health Organization; 2018 p. 106.
5. WHO. Global leprosy (Hansen disease) update, 2019: time to step-up prevention initiatives. *Wkly Epidemiol Rec*. 2020; 95: 417–440.
6. Nath I, Saini C, Valluri VL. Immunology of leprosy and diagnostic challenges. *Clin Dermatol*. 2015; 33: 90–98. <https://doi.org/10.1016/j.clindermatol.2014.07.005> PMID: [25432814](https://pubmed.ncbi.nlm.nih.gov/25432814/)
7. van Hooij A, Tjon Kon Fat EM, Batista da Silva M, Carvalho Bouth R, Cunha Messias AC, Gobbo AR, et al. Evaluation of Immunodiagnostic Tests for Leprosy in Brazil, China and Ethiopia. *Sci Rep*. 2018; 8: 1–9. <https://doi.org/10.1038/s41598-017-17765-5> PMID: [29311619](https://pubmed.ncbi.nlm.nih.gov/29311619/)
8. van Hooij A, van den Eeden S, Richardus R, Tjon Kon Fat E, Wilson L, Franken KLMC, et al. Application of new host biomarker profiles in quantitative point-of-care tests facilitates leprosy diagnosis in the field. *EBioMedicine*. 2019; 47: 301–308. <https://doi.org/10.1016/j.ebiom.2019.08.009> PMID: [31422044](https://pubmed.ncbi.nlm.nih.gov/31422044/)
9. Manta FS de N, Leal-Calvo T, Moreira SJM, Marques BLC, Ribeiro-Alves M, Rosa PS, et al. Ultra-sensitive detection of *Mycobacterium leprae*: DNA extraction and PCR assays. Poonawala H, editor. *PLoS Negl Trop Dis*. 2020; 14: e0008325. <https://doi.org/10.1371/journal.pntd.0008325> PMID: [32453754](https://pubmed.ncbi.nlm.nih.gov/32453754/)
10. Gliddon HD, Herberg JA, Levin M, Kafrou M. Genome-wide host RNA signatures of infectious diseases: discovery and clinical translation. *Immunology*. 2018; 153: 171–178. <https://doi.org/10.1111/imm.12841> PMID: [28921535](https://pubmed.ncbi.nlm.nih.gov/28921535/)

11. Ko ER, Yang WE, McClain MT, Woods CW, Ginsburg GS, Tsalik EL. What was old is new again: Using the host response to diagnose infectious disease. *Expert Rev Mol Diagn.* 2015; 15: 1143–1158. <https://doi.org/10.1586/14737159.2015.1059278> PMID: 26145249
12. Miller RR, Lopansri BK, Burke JP, Levy M, Opal S, Rothman RE, et al. Validation of a host response assay, SeptiCyte LAB, for discriminating sepsis from systemic inflammatory response syndrome in the ICU. *Am J Respir Crit Care Med.* 2018; 198: 903–913. <https://doi.org/10.1164/rccm.201712-2472OC> PMID: 29624409
13. Van Hooij A, Fat EMTK, Van Den Eeden SJF, Wilson L, Da Silva MB, Salgado CG, et al. Field-friendly serological tests for determination of *M. Leprae*-specific antibodies. *Sci Rep.* 2017; 7: 1–8. <https://doi.org/10.1038/s41598-016-0028-x> PMID: 28127051
14. Warsinske H, Vashisht R, Khatri P. Host-response-based gene signatures for tuberculosis diagnosis: A systematic comparison of 16 signatures. *PLoS Med.* 2019; 16. <https://doi.org/10.1371/journal.pmed.1002786> PMID: 31013272
15. Röltgen K, Pluschke G, Spencer JS, Brennan PJ, Avanzi C. The immunology of other mycobacteria: *M. ulcerans*, *M. leprae*. *Semin Immunopathol.* 2020; 42: 333–353. <https://doi.org/10.1007/s00281-020-00790-4> PMID: 32100087
16. Mesko B, Poliska S, Nagy L. Gene expression profiles in peripheral blood for the diagnosis of autoimmune diseases. *Trends Mol Med.* 2011; 17: 223–233. <https://doi.org/10.1016/j.molmed.2010.12.004> PMID: 21388884
17. Wang B, Chen S, Zheng Q, Gao Z, Chen R, Xuan J, et al. Development and initial validation of diagnostic gene signatures for systemic lupus erythematosus. *Ann Rheum Dis.* 2019. <https://doi.org/10.1136/annrheumdis-2019-216695> PMID: 31811057
18. Carlson JJ, Roth JA. The impact of the Oncotype Dx breast cancer assay in clinical practice: A systematic review and meta-analysis. *Breast Cancer Res Treat.* 2013; 141: 13–22. <https://doi.org/10.1007/s10549-013-2666-z> PMID: 23974828
19. Gordon GJ, Jensen RV, Hsiao LL, Gullans SR, Blumenstock JE, Ramaswamy S, et al. Translation of microarray data into clinically relevant cancer diagnostic tests using gene expression ratios in lung cancer and mesothelioma. *Cancer Res.* 2002; 62: 4963–4967. PMID: 12208747
20. Narrandes S, Xu W. Gene expression detection assay for cancer clinical use. *J Cancer.* 2018; 9: 2249–2265. <https://doi.org/10.7150/jca.24744> PMID: 30026820
21. Clark-Langone KM, Sangli C, Krishnakumar J, Watson D. Translating tumor biology into personalized treatment planning: analytical performance characteristics of the Oncotype DX Colon Cancer Assay. *BMC Cancer.* 2010; 10: 691. <https://doi.org/10.1186/1471-2407-10-691> PMID: 21176237
22. Knezevic D, Goddard AD, Natraj N, Cherbavaz DB, Clark-Langone KM, Snable J, et al. Analytical validation of the Oncotype DX prostate cancer assay—a clinical RT-PCR assay optimized for prostate needle biopsies. *BMC Genomics.* 2013; 14: 1–12. <https://doi.org/10.1186/1471-2164-14-1> PMID: 23323973
23. Laible M, Schlombs K, Kaiser K, Veltrup E, Herlein S, Lakis S, et al. Technical validation of an RT-qPCR in vitro diagnostic test system for the determination of breast cancer molecular subtypes by quantification of ERBB2, ESR1, PGR and MKI67 mRNA levels from formalin- fixed paraffin-embedded breast tumor specimens. *BMC Cancer.* 2016; 1–14. <https://doi.org/10.1186/s12885-016-2476-x> PMID: 27389414
24. Belone A de FF, Rosa PS, Trombone APF, Fachin LRV, Guidella CC, Ura S, et al. Genome-wide screening of mRNA expression in leprosy patients. *Front Genet.* 2015; 6: 1–12. <https://doi.org/10.3389/fgene.2015.00001> PMID: 25674101
25. Jorge KTOS Souza RP, Assis MTA Araújo MG, Locati M Jesus AMR, et al. Characterization of MicroRNA Expression Profiles and Identification of Potential Biomarkers in Leprosy. *J Clin Microbiol.* 2017; 55: 1516–1525. <https://doi.org/10.1128/JCM.02408-16> PMID: 28275081
26. Tió-Coma M, van Hooij A, Bobosha K, van der Ploeg-van Schip JJ, Banu S, Khadge S, et al. Whole blood RNA signatures in leprosy patients identify reversal reactions before clinical onset: a prospective, multicenter study. *Sci Rep.* 2019; 9: 17931. <https://doi.org/10.1038/s41598-019-54213-y> PMID: 31784594
27. Tió-Coma M, Kielbasa SM, van den Eeden SJF, Mei H, Roy JC, Wallinga J, et al. Blood RNA signature RISK4LEP predicts leprosy years before clinical onset. *EBioMedicine.* 2021; 68: 103379. <https://doi.org/10.1016/j.ebiom.2021.103379> PMID: 34090257
28. Montoya DJ, Andrade P, Silva BJA, Teles RMB, Ma F, Bryson B, et al. Dual RNA-Seq of Human Leprosy Lesions Identifies Bacterial Determinants Linked to Host Immune Response. *Cell Rep.* 2019; 26: 3574–3585.e3. <https://doi.org/10.1016/j.celrep.2019.02.109> PMID: 30917313
29. Bhatia S, Shenoi SD, Pai K, Srilatha PS. Granuloma multiforme: an uncommon differential for leprosy. *Trop Doct.* 2019; 49: 55–58. <https://doi.org/10.1177/0049475518803191> PMID: 30286700

30. Kundakci N, Erdem C. Leprosy: A great imitator. *Clin Dermatol*. 2019; 37: 200–212. <https://doi.org/10.1016/j.clindermatol.2019.01.002> PMID: 31178103
31. Zhu TH, Kamangar F, Silverstein M, Fung MA. Borderline Tuberculoid Leprosy Masquerading as Granuloma Annulare: A Clinical and Histological Pitfall. *Am J Dermatopathol*. 2017; 39: 296–299. <https://doi.org/10.1097/DAD.0000000000000698> PMID: 28328616
32. Blischak JD, Tailleux L, Mitrano A, Barreiro LB, Gilad Y. Mycobacterial infection induces a specific human innate immune response. *Sci Rep*. 2015; 5: 1–16. <https://doi.org/10.1038/srep16882> PMID: 26586179
33. Modlin RL. Th1-Th2 paradigm: insights from leprosy. *J Invest Dermatol*. 1994; 102: 828–832. <https://doi.org/10.1111/1523-1747.ep12381958> PMID: 8006444
34. Yamamura M, Uyemura K, Deans RJ, Weinberg K, Rea TH, Bloom BR, et al. Defining protective responses to pathogens: Cytokine profiles in leprosy lesions. *Science*. 1991; 254: 277–279. <https://doi.org/10.1126/science.254.5029.277> PMID: 1925582
35. Leal-Calvo T, Moraes MO. Reanalysis and integration of public microarray datasets reveals novel host genes modulated in leprosy. *Mol Genet Genomics*. 2020; 295: 1355–1368. <https://doi.org/10.1007/s00438-020-01705-6> PMID: 32661593
36. Judson MA, Marchell RM, Mascelli M, Piantone A, Barnathan ES, Petty KJ, et al. Molecular profiling and gene expression analysis in cutaneous sarcoidosis: the role of interleukin-12, interleukin-23, and the T-helper 17 pathway. *J Am Acad Dermatol*. 2012; 66: 901–910, 910.e1–2. <https://doi.org/10.1016/j.jaad.2011.06.017> PMID: 21924794
37. Linke M, Pham HTT, Katholnig K, Schnöller T, Miller A, Demel F, et al. Chronic signaling via the metabolic checkpoint kinase mTORC1 induces macrophage granuloma formation and marks sarcoidosis progression. *Nat Immunol*. 2017; 18: 293–302. <https://doi.org/10.1038/ni.3655> PMID: 28092373
38. Masaki T, Qu J, Cholewa-Waclaw J, Burr K, Raam R, Rambukkana A. Reprogramming adult Schwann cells to stem cell-like cells by leprosy bacilli promotes dissemination of infection. *Cell*. 2013; 152: 51–67. <https://doi.org/10.1016/j.cell.2012.12.014> PMID: 23332746
39. Brabletz T, Kalluri R, Nieto MA, Weinberg RA. EMT in cancer. *Nat Rev Cancer*. 2018; 18: 128–134. <https://doi.org/10.1038/nrc.2017.118> PMID: 29326430
40. Pastushenko I, Blanpain C. EMT Transition States during Tumor Progression and Metastasis. *Trends Cell Biol*. 2019; 29: 212–226. <https://doi.org/10.1016/j.tcb.2018.12.001> PMID: 30594349
41. Khazai Z, Van Brakel W, Essink D, Gillis T, Kasang C, Kuipers P, et al. Reviewing Research Priorities of the Leprosy Research Initiative (LRI): a stakeholder's consultation. *Lepr Rev*. 2019; 90: 3–30. <https://doi.org/10.47276/lr.90.1.3>
42. Chen W. IDO: more than an enzyme. *Nat Immunol*. 2011; 12: 809–811. <https://doi.org/10.1038/ni.2088> PMID: 21852775
43. Greco FA, Coletti A, Camaioni E, Carotti A, Marinozzi M, Gioiello A, et al. The Janus-faced nature of IDO1 in infectious diseases: challenges and therapeutic opportunities. *Future Med Chem*. 2016; 8: 39–54. <https://doi.org/10.4155/fmc.15.165> PMID: 26692277
44. Melé M, Ferreira PG, Reverter F, DeLuca DS, Monlong J, Sammeth M, et al. The human transcriptome across tissues and individuals. *Science*. 2015; 348: 660–665. <https://doi.org/10.1126/science.aaa0355> PMID: 25954002
45. Yamazaki F, Kuroiwa T, Takikawa O, Kido R. Human indolylamine 2,3-dioxygenase. Its tissue distribution, and characterization of the placental enzyme. *Biochem J*. 1985; 230: 635–638. <https://doi.org/10.1042/bj2300635> PMID: 3877502
46. Hughes TK, Wadsworth MH, Gierahn TM, Do T, Weiss D, Andrade PR, et al. Second-Strand Synthesis-Based Massively Parallel scRNA-Seq Reveals Cellular States and Molecular Features of Human Inflammatory Skin Pathologies. *Immunity*. 2020; 53: 878–894.e7. <https://doi.org/10.1016/j.immuni.2020.09.015> PMID: 33053333
47. Gautam US, Foreman TW, Bucsan AN, Veatch AV, Alvarez X, Adekambi T, et al. In vivo inhibition of tryptophan catabolism reorganizes the tuberculoma and augments immune-mediated control of Mycobacterium tuberculosis. *Proc Natl Acad Sci U S A*. 2018; 115: E62–E71. <https://doi.org/10.1073/pnas.1711373114> PMID: 29255022
48. Yeung AWS, Terentis AC, King NJC, Thomas SR. Role of indoleamine 2,3-dioxygenase in health and disease. *Clin Sci*. 2015; 129: 601–672. <https://doi.org/10.1042/CS20140392> PMID: 26186743
49. Denys A, Allain F. The emerging roles of heparan sulfate 3-O-sulfotransferases in cancer. *Front Oncol*. 2019;9. <https://doi.org/10.3389/fonc.2019.00507> PMID: 31249810
50. Yamauchi PS, Bleharski JR, Uyemura K, Kim J, Sieling PA, Miller A, et al. A Role for CD40-CD40 Ligand Interactions in the Generation of Type 1 Cytokine Responses in Human Leprosy. *J Immunol*. 2000; 165: 1506–1512. <https://doi.org/10.4049/jimmunol.165.3.1506> PMID: 10903757

51. Heim A. Highly sensitive detection of gene expression of an intronless gene: amplification of mRNA, but not genomic DNA by nucleic acid sequence based amplification (NASBA). *Nucleic Acids Res.* 1998; 26: 2250–2251. <https://doi.org/10.1093/nar/26.9.2250> PMID: 9547289
52. Patterson SS, Casper ET, Garcia-Rubio L, Smith MC, Paul JH. Increased precision of microbial RNA quantification using NASBA with an internal control. *J Microbiol Methods.* 2005; 60: 343–352. <https://doi.org/10.1016/j.mimet.2004.10.011> PMID: 15649536
53. Ganguli A, Ornob A, Spegazzini N, Liu Y, Damhorst G, Ghonge T, et al. Pixelated spatial gene expression analysis from tissue. *Nat Commun.* 2018; 9. <https://doi.org/10.1038/s41467-017-02623-9> PMID: 29335461
54. Pandey M, Singh D, Onteru SK. Reverse transcription loop-mediated isothermal amplification (RT-LAMP), a light for mammalian transcript analysis in low-input laboratories. *J Cell Biochem.* 2018; 119: 4334–4338. <https://doi.org/10.1002/jcb.26624> PMID: 29266331
55. Broughton JP, Deng X, Yu G, Fasching CL, Servellita V, Singh J, et al. CRISPR–Cas12-based detection of SARS-CoV-2. *Nat Biotechnol.* 2020; 38: 870–874. <https://doi.org/10.1038/s41587-020-0513-4> PMID: 32300245
56. Barbieri RR, Manta FSN, Moreira SJM, Sales AM, Nery JAC, Nascimento LPR, et al. Quantitative polymerase chain reaction in paucibacillary leprosy diagnosis: A follow-up study. *PLoS Negl Trop Dis.* 2019; 13: e0007147. <https://doi.org/10.1371/journal.pntd.0007147> PMID: 30835722
57. Strassner JP, Rashighi M, Ahmed Refat M, Richmond JM, Harris JE. Suction blistering the lesional skin of vitiligo patients reveals useful biomarkers of disease activity. *J Am Acad Dermatol.* 2017; 76: 847–855.e5. <https://doi.org/10.1016/j.jaad.2016.12.021> PMID: 28259440
58. Elamin AA, Stehr M, Singh M. Lipid Droplets and Mycobacterium leprae Infection. *J Pathog.* 2012; 10. <https://doi.org/10.1155/2012/361374> PMID: 23209912
59. Lobato LS, Rosa PS, Ferreira J da S, Neumann A da S, da Silva MG, do Nascimento DC, et al. Statins increase rifampin mycobactericidal effect. *Antimicrob Agents Chemother.* 2014; 58: 5766–74. <https://doi.org/10.1128/AAC.01826-13> PMID: 25049257
60. Wang D, Zhang D-F, Li G-D, Bi R, Fan Y, Wu Y, et al. A pleiotropic effect of the APOE gene: association of APOE polymorphisms with multibacillary leprosy in Han Chinese from Southwest China. *Br J Dermatol.* 2018; 178: 931–939. <https://doi.org/10.1111/bjd.16020> PMID: 28977675
61. Fabel A, Giovanna Brunasso AM, Schettini AP, Cota C, Puntoni M, Nunzi E, et al. Pathogenesis of Leprosy. *Am J Dermatopathol.* 2019; 41: 422–427. <https://doi.org/10.1097/DAD.0000000000001310> PMID: 30422829
62. Iyer AM, Mohanty KK, van Egmond D, Katoch K, Faber WR, Das PK, et al. Leprosy-specific B-cells within cellular infiltrates in active leprosy lesions. *Hum Pathol.* 2007; 38: 1065–1073. <https://doi.org/10.1016/j.humpath.2006.12.017> PMID: 17442378
63. Medeiros RCA, Girardi K do C de V, Cardoso FKL, Mietto B de S, Pinto TG de T, Gomez LS, et al. Subversion of Schwann Cell Glucose Metabolism by Mycobacterium leprae. *J Biol Chem.* 2016; 291: 21375–21387. <https://doi.org/10.1074/jbc.M116.725283> PMID: 27555322
64. de Toledo-Pinto TG, Ferreira ABR, Ribeiro-Alves M, Rodrigues LS, Batista-Silva LR, Silva BJ de A, et al. STING-Dependent 2'-5' Oligoadenylate Synthetase-Like Production Is Required for Intracellular Mycobacterium leprae Survival. *J Infect Dis.* 2016; 214: 311–320. <https://doi.org/10.1093/infdis/jiw144> PMID: 27190175
65. Hess S, Rambukkana A. Bacterial-induced cell reprogramming to stem cell-like cells: new premise in host–pathogen interactions. *Curr Opin Microbiol.* 2015; 23: 179–188. <https://doi.org/10.1016/j.mib.2014.11.021> PMID: 25541240
66. Vandewalle C, Comijn J, De Craene B, Vermassen P, Bruyneel E, Andersen H, et al. SIP1/ZEB2 induces EMT by repressing genes of different epithelial cell-cell junctions. *Nucleic Acids Res.* 2005; 33: 6566–6578. <https://doi.org/10.1093/nar/gki965> PMID: 16314317
67. DaSilva-Arnold SC, Kuo CY, Davra V, Remache Y, Kim PCW, Fisher JP, et al. ZEB2, a master regulator of the epithelial-mesenchymal transition, mediates trophoblast differentiation. *Mol Hum Reprod.* 2018; 25: 61–75. <https://doi.org/10.1093/molehr/gay053> PMID: 30462321
68. Jiang Y, Zhou J, Hou D, Luo P, Gao H, Ma Y, et al. Prosaposin is a biomarker of mesenchymal glioblastoma and regulates mesenchymal transition through the TGF- β 1/Smad signaling pathway. *J Pathol.* 2019; 249: 26–38. <https://doi.org/10.1002/path.5278> PMID: 30953361
69. Frugtniet BA, Martin TA, Zhang L, Jiang WG. Neural Wiskott-Aldrich syndrome protein (nWASP) is implicated in human lung cancer invasion. *BMC Cancer.* 2017; 17. <https://doi.org/10.1186/s12885-016-3000-z> PMID: 28056866
70. Bendris N, Arsic N, Lemmers B, Blanchard JM. Cyclin A2, Rho GTPases and EMT. *Small GTPases.* 2012; 3: 225–228. <https://doi.org/10.4161/sgtp.20791> PMID: 22735340

71. Bhowmick NA, Ghiassi M, Bakin A, Aakre M, Lundquist CA, Engel ME, et al. Transforming growth factor- β 1 mediates epithelial to mesenchymal transdifferentiation through a RhoA-dependent mechanism. *Mol Biol Cell*. 2001; 12: 27–36. <https://doi.org/10.1091/mbc.12.1.27> PMID: 11160820
72. Salvi A, Thanabalu T. WIP promotes in-vitro invasion ability, anchorage independent growth and EMT progression of A549 lung adenocarcinoma cells by regulating RhoA levels. *Biochem Biophys Res Commun*. 2017; 482: 1353–1359. <https://doi.org/10.1016/j.bbrc.2016.12.040> PMID: 27939884
73. Wang Q, Yang X, Xu Y, Shen Z, Cheng H, Cheng F, et al. RhoA/Rho-kinase triggers epithelial-mesenchymal transition in mesothelial cells and contributes to the pathogenesis of dialysis-related peritoneal fibrosis. *Oncotarget*. 2018; 9: 14397–14412. <https://doi.org/10.18632/oncotarget.24208> PMID: 29581852
74. Wang J, Chen L, Li Y, Guan XY. Overexpression of cathepsin Z contributes to tumor metastasis by inducing epithelial-mesenchymal transition in hepatocellular carcinoma. *PLoS ONE*. 2011; 6. <https://doi.org/10.1371/journal.pone.0024967> PMID: 21966391
75. Lin CY, Tsai PH, Kandaswami CC, Lee PP, Huang CJ, Hwang JJ, et al. Matrix metalloproteinase-9 cooperates with transcription factor Snail to induce epithelial-mesenchymal transition. *Cancer Sci*. 2011; 102: 815–827. <https://doi.org/10.1111/j.1349-7006.2011.01861.x> PMID: 21219539
76. Peinado H, del Carmen Iglesias-de la Cruz M, Olmeda D, Csiszar K, Fong KSK, Vega S, et al. A molecular role for lysyl oxidase-like 2 enzyme in Snail regulation and tumor progression. *EMBO J*. 2005; 24: 3446–3458. <https://doi.org/10.1038/sj.emboj.7600781> PMID: 16096638
77. Tam SY, Wu VWC, Law HKW. Hypoxia-Induced Epithelial-Mesenchymal Transition in Cancers: HIF-1 α and Beyond. *Front Oncol*. 2020; 10. <https://doi.org/10.3389/fonc.2020.00486> PMID: 32322559
78. Zhu Y, Tan J, Xie H, Wang J, Meng X, Wang R. HIF-1 α regulates EMT via the Snail and β -catenin pathways in paraquat poisoning-induced early pulmonary fibrosis. *J Cell Mol Med*. 2016; 20: 688–697. <https://doi.org/10.1111/jcmm.12769> PMID: 26781174
79. Lyrio ECD, Campos-Souza IC, Corrêa LCD, Lechuga GC, Verícimo M, Castro HC, et al. Interaction of *Mycobacterium leprae* with the HaCaT human keratinocyte cell line: new frontiers in the cellular immunology of leprosy. *Exp Dermatol*. 2015; 24: 536–542. <https://doi.org/10.1111/exd.12714> PMID: 25828729
80. Okada S, Komura J, Nishiura M. *Mycobacterium leprae* found in epidermal cells by electron microscopy. *IntJLeprOther MycobactDis*. 1978; 46: 30–34. PMID: 348610
81. Pivarcsi A, Kemény L, Dobozy A. Innate Immune Functions of the Keratinocytes. *Acta Microbiol Immunol Hung*. 2004; 51: 303–310. <https://doi.org/10.1556/AMicr.51.2004.3.8> PMID: 15571070
82. Pivarcsi A, Nagy I, Lajos K. Innate Immunity in the Skin: How Keratinocytes Fight Against Pathogens. *Curr Immunol Rev*. 2005; 1: 29–43. <https://doi.org/10.2174/1573395052952941>
83. Damsky W, Thakral D, McGeary MK, Leventhal J, Galan A, King B. Janus kinase inhibition induces disease remission in cutaneous sarcoidosis and granuloma annulare. *J Am Acad Dermatol*. 2020; 82: 612–621. <https://doi.org/10.1016/j.jaad.2019.05.098> PMID: 31185230
84. Flynn JL, Chan J, Lin PL. Macrophages and control of granulomatous inflammation in tuberculosis. *Mucosal Immunol*. 2011; 4: 271–278. <https://doi.org/10.1038/mi.2011.14> PMID: 21430653
85. Locke LW, Crouser ED, White P, Julian MW, Caceres EG, Papp AC, et al. IL-13–regulated Macrophage Polarization during Granuloma Formation in an In Vitro Human Sarcoidosis Model. *Am J Respir Cell Mol Biol*. 2019; 60: 84–95. <https://doi.org/10.1165/rcmb.2018-0053OC> PMID: 30134122
86. Manta FSN, Barbieri RR, Moreira SJM, Santos PTS, Nery JAC, Duppre NC, et al. Quantitative PCR for leprosy diagnosis and monitoring in household contacts: A follow-up study, 2011–2018. *Sci Rep*. 2019; 9. <https://doi.org/10.1038/s41598-019-52640-5> PMID: 31723144
87. Brabham Bioinformatics. FastQC: A Quality Control Tool for High Throughput Sequence Data [Online]. 2015. Available: <http://www.bioinformatics.babraham.ac.uk/projects/fastqc/>
88. Patro R, Duggal G, Love MI, Irizarry RA, Kingsford C. Salmon provides fast and bias-aware quantification of transcript expression. *Nat Methods*. 2017; 14: 417–419. <https://doi.org/10.1038/nmeth.4197> PMID: 28263959
89. R Core Team. R: A language and environment for statistical computing. Vienna, Austria; 2017. Available: <https://www.r-project.org/>
90. Sonesson C, Love MI, Robinson MD. Differential analyses for RNA-seq: transcript-level estimates improve gene-level inferences. *F1000Research*. 2016; 4: 1521. <https://doi.org/10.12688/f1000research.7563.2> PMID: 26925227
91. Durinck S, Moreau Y, Kasprzyk A, Davis S, De Moor B, Brazma A, et al. BioMart and Bioconductor: a powerful link between biological databases and microarray data analysis. *Bioinformatics*. 2005; 21: 3439–3440. <https://doi.org/10.1093/bioinformatics/bti525> PMID: 16082012

92. Anders S, Huber W. Differential expression analysis for sequence count data. *Genome Biol.* 2010; 11: R106. <https://doi.org/10.1186/gb-2010-11-10-r106> PMID: 20979621
93. Love MI, Huber W, Anders S. Moderated estimation of fold change and dispersion for RNA-seq data with DESeq2. *Genome Biol.* 2014; 15: 550. <https://doi.org/10.1186/s13059-014-0550-8> PMID: 25516281
94. Zhu A, Ibrahim JG, Love MI. Heavy-Tailed prior distributions for sequence count data: Removing the noise and preserving large differences. *Bioinformatics.* 2019; 35: 2084–2092. <https://doi.org/10.1093/bioinformatics/bty895> PMID: 30395178
95. Gagnon-Bartsch JA, Speed TP. Using control genes to correct for unwanted variation in microarray data. *Biostatistics.* 2012; 13: 539–552. <https://doi.org/10.1093/biostatistics/kxr034> PMID: 22101192
96. Risso D, Ngai J, Speed TP, Dudoit S. Normalization of RNA-seq data using factor analysis of control genes or samples. *Nat Biotechnol.* 2014; 32: 896–902. <https://doi.org/10.1038/nbt.2931> PMID: 25150836
97. Benjamini Y, Hochberg Y. Controlling the False Discovery Rate: A Practical and Powerful Approach to Multiple Testing. *Journal of the Royal Statistical Society. Series B (Methodological)*. WileyRoyal Statistical Society; 1995. <https://doi.org/10.2307/2346101>
98. Phipson B, Lee S, Majewski IJ, Alexander WS, Smyth GK. Robust hyperparameter estimation protects against hypervariable genes and improves power to detect differential expression. *Ann Appl Stat.* 2016; 10: 946–963. <https://doi.org/10.1214/16-AOAS920> PMID: 28367255
99. Ritchie ME, Phipson B, Wu D, Hu Y, Law CW, Shi W, et al. limma powers differential expression analyses for RNA-sequencing and microarray studies. *Nucleic Acids Res.* 2015; 43: e47. <https://doi.org/10.1093/nar/gkv007> PMID: 25605792
100. Smyth GK. Linear Models and Empirical Bayes Methods for Assessing Differential Expression in Microarray Experiments Linear Models and Empirical Bayes Methods for Assessing Differential Expression in Microarray Experiments. *Stat Appl Genet Mol Biol.* 2004; 3: 1–26. <https://doi.org/10.2202/1544-6115.1027> PMID: 16646809
101. Wickham H. ggplot2-Elegant Graphics for Data Analysis. 1st ed. New York, NY: Springer New York; 2009. <https://doi.org/10.1007/978-0-387-98141-3>
102. Gu Z, Eils R, Schlesner M. Complex heatmaps reveal patterns and correlations in multidimensional genomic data. *Bioinformatics.* 2016; 32: 2847–2849. <https://doi.org/10.1093/bioinformatics/btw313> PMID: 27207943
103. Kolde R. pheatmap: Pretty Heatmaps. 2015. Available: <https://cran.r-project.org/package=pheatmap>
104. Yu G, Wang L-G, Han Y, He Q-Y. clusterProfiler: an R Package for Comparing Biological Themes Among Gene Clusters. *OMICS J Integr Biol.* 2012; 16: 284–287. <https://doi.org/10.1089/omi.2011.0118> PMID: 22455463
105. Carlson M. org.Hs.eg.db: Genome wide annotation for Human. 2019. Available: <https://doi.org/10.18129/B9.bioc.org.Hs.eg.db>
106. Koressaar T, Remm M. Enhancements and modifications of primer design program Primer3. *Bioinformatics.* 2007; 23: 1289–1291. <https://doi.org/10.1093/bioinformatics/btm091> PMID: 17379693
107. Kõressaar T, Lepamets M, Kaplinski L, Raime K, Andreson R, Remm M. Primer3_masker: integrating masking of template sequence with primer design software. *Bioinformatics.* 2018; 34: 1937–1938. <https://doi.org/10.1093/bioinformatics/bty036> PMID: 29360956
108. Untergasser A, Cutcutache I, Koressaar T, Ye J, Faircloth BC, Remm M, et al. Primer3—new capabilities and interfaces. *Nucleic Acids Res.* 2012; 40: e115–e115. <https://doi.org/10.1093/nar/gks596> PMID: 22730293
109. Ye J, Coulouris G, Zaretskaya I, Cutcutache I, Rozen S, Madden TL. Primer-BLAST: a tool to design target-specific primers for polymerase chain reaction. *BMC Bioinformatics.* 2012; 13: 134. <https://doi.org/10.1186/1471-2105-13-134> PMID: 22708584
110. Qu W, Shen Z, Zhao D, Yang Y, Zhang C. MFEprimer: Multiple factor evaluation of the specificity of PCR primers. *Bioinformatics.* 2009; 25: 276–278. <https://doi.org/10.1093/bioinformatics/btn614> PMID: 19038987
111. Wang K, Li H, Xu Y, Shao Q, Yi J, Wang R, et al. MFEprimer-3.0: Quality control for PCR primers. *Nucleic Acids Res.* 2019; 47: W610–W613. <https://doi.org/10.1093/nar/gkz351> PMID: 31066442
112. Ramakers C, Ruijter JM, Lekanne Deprez RH, Moorman AFM. Assumption-free analysis of quantitative real-time polymerase chain reaction (PCR) data. *Neurosci Lett.* 2003; 339: 62–66. [https://doi.org/10.1016/s0304-3940\(02\)01423-4](https://doi.org/10.1016/s0304-3940(02)01423-4) PMID: 12618301
113. Ruijter JM, Ramakers C, Hoogaars WMH, Karlen Y, Bakker O, Van den hoff MJB, et al. Amplification efficiency: Linking baseline and bias in the analysis of quantitative PCR data. *Nucleic Acids Res.* 2009; 37. <https://doi.org/10.1093/nar/gkp045> PMID: 19237396

114. Vandesompele J, De Preter K, Pattyn ilip, Poppe B, Van Roy N, De Paepe A, et al. Accurate normalization of real-time quantitative RT-PCR data by geometric averaging of multiple internal control genes. *Genome Biol.* 2002; 3: 34–1. <https://doi.org/10.1186/gb-2002-3-7-research0034> PMID: 12184808
115. Matz MV, Wright RM, Scott JG. No control genes required: Bayesian analysis of qRT-PCR data. *PLoS One.* 2013; 8: 1–12. <https://doi.org/10.1371/journal.pone.0071448> PMID: 23977043
116. Steibel JP, Poletto R, Coussens PM, Rosa GJM. A powerful and flexible linear mixed model framework for the analysis of relative quantification RT-PCR data. *Genomics.* 2009; 94: 146–152. <https://doi.org/10.1016/j.ygeno.2009.04.008> PMID: 19422910
117. Fieller EC, Hartley HO, Pearson ES. TESTS FOR RANK CORRELATION COEFFICIENTS I. *Biometrika.* 1957; 44: 470–481. <https://doi.org/10.1093/biomet/44.3-4.470>
118. Makowski D, Ben-Shachar MS, Patil I, Lüdecke D. Methods and Algorithms for Correlation Analysis in R. *J Open Source Softw.* 2020; 5: 2306. <https://doi.org/10.21105/joss.02306>
119. Friedman J, Hastie T, Tibshirani R. Regularization paths for generalized linear models via coordinate descent. *J Stat Softw.* 2010; 33: 1–22. <https://doi.org/10.18637/jss.v033.i01> PMID: 20808728
120. Simon N, Friedman JH, Hastie T, Tibshirani R. Regularization Paths for Cox's Proportional Hazards Model via Coordinate Descent. *J Stat Softw.* 2011; 39: 1–13. <https://doi.org/10.18637/jss.v039.i05> PMID: 27065756
121. Tibshirani R. Regression Shrinkage and Selection via the Lasso. *J R Stat Soc Ser B Methodol.* 1996; 58: 267–288.
122. Hastie T, Tibshirani R, Wainwright M. *Statistical Learning with Sparsity.* 1st ed. Chapman and Hall/CRC; 2015.
123. Davison AC, Hinley DV. *Bootstrap Methods and Their Application.* Cambridge University Press; 1997. Available: <http://statwww.epfl.ch/davison/BMA/>
124. DeLong ER, DeLong DM, Clarke-Pearson DL. Comparing the Areas under Two or More Correlated Receiver Operating Characteristic Curves: A Nonparametric Approach. *Biometrics.* 1988; 44: 837. <https://doi.org/10.2307/2531595> PMID: 3203132
125. Robin X, Turck N, Hainard A, Tiberti N, Lisacek F, Sanchez JC, et al. pROC: An open-source package for R and S+ to analyze and compare ROC curves. *BMC Bioinformatics.* 2011; 12: 77. <https://doi.org/10.1186/1471-2105-12-77> PMID: 21414208
126. Sun X, Xu W. Fast implementation of DeLong's algorithm for comparing the areas under correlated receiver operating characteristic curves. *IEEE Signal Process Lett.* 2014; 21: 1389–1393. <https://doi.org/10.1109/LSP.2014.2337313>